Energy 185 (2019) 744–762

Contents lists available at ScienceDirect

Energy

journal homepage: www.elsevier.com/locate/energy

Gain scheduling design based on active disturbance rejection control for thermal power plant under full operating conditions

Zhenlong Wu [a], Donghai Li [a, *], Yali Xue [a], YangQuan Chen [b]

[a] State Key Lab of Power Systems, Department of Energy and Power Engineering, Tsinghua University, Beijing, 100084, PR China
[b] Mechatronics, Embedded Systems and Automation (MESA) Lab, School of Engineering, University of California, Merced, CA, 95343, USA

ARTICLE INFO

Article history:
Received 22 October 2018
Received in revised form
1 July 2019
Accepted 11 July 2019
Available online 12 July 2019

Keywords:
Gain scheduling
Active disturbance rejection control
Coordinated control system
Full operating conditions
Stability analysis

ABSTRACT

To integrate more renewable energy into the power grid, thermal power plants have to accelerate the speed of power output and extend their operating ranges, and this can result in great challenges for their safe operations and even safety accidents. To this end, a gain scheduling design based on active disturbance rejection control (ADRC) is proposed for thermal power plants under full operating conditions. The urgency of the proposed control strategy is illustrated by analyzing the control difficulties of coordinated control systems. Then the scheduling parameter selection and the linear switching method for the proposed control strategy are analyzed. Moreover, the qualitative stability analysis based on the Kharitonov theorem and the quantitative calculation of stability regions are carried out to ensure the stability of the closed-loop system. Simulations of the power tracking under different load tracking rates and disturbance rejection under the coal quality variation are carried out. Simulation results show that the tracking and disturbance rejection performance in both power output and throttle pressure loops has been improved simultaneously compared with the regular ADRC and the traditional proportional-integral control strategies. Based on the verified superiority, the proposed gain scheduling design based on ADRC shows a promising potential in industrial applications.

1. Introduction

With the booming growth of the renewable energy such as solar, wind and tidal power generation in the electricity market, the safety operation of power grid is becoming a challenging issue [1]. The increased impact from these fluctuating energy sources which have strong intermittency and randomness significantly affects the operational regime of thermal power plants that have to accelerate the speed of power output responding the automatic generation control (AGC) command and extend the operating range [2]. The frequent and extensive load changes can result in severe thermo-mechanical fatigue, creep and corrosion which can cause a life-time reduction [3,4]. Besides, strict control requirements for the efficiency and safety put forward great challenges of the management strategies of thermal power plants, especially the daily operational strategies. The proportional-integral/proportional-integral-derivative (PI/PID) controllers still dominate the industry (more than 98% of all power plant controllers in Guangdong Province, China) and undoubtedly play a key role in current thermal processes [5]. However, facing with strong nonlinear characteristics, strong cross-coupling, wide operating conditions and strict control requirements, the traditional control strategy cannot obtain the satisfactory control performance [6].

To research dynamic characteristics of thermal power plants, a dynamic power plant model with an innovative level of detail is developed and the model can be used to optimize start-up costs and environmental impact [7]. Dynamic models of combined cycle power plants are also proposed to predict the thermodynamic variables trend so that the lifetime reduction of the power plants can be assessed [8,9]. A model of three pressure level heat recovery steam generator is proposed to estimate the most stressed devices lifetime reduction [10]. Besides, a model of organic Rankine cycle units is built to analyze hot spots in boilers during transient operation [11]. An experiment-based model of condensate throttling for 1000 MW power units is developed to analyze the dynamic of storage energy [12]. To design better control strategies based on the dynamic model of power plants, some nonlinear dynamic models are built recently. Åström develops a famous nonlinear dynamic model for natural circulation drum-boilers which is intend for

* Corresponding author.
E-mail address: lidongh@mail.tsinghua.edu.cn (D. Li).

https://doi.org/10.1016/j.energy.2019.07.077
0360-5442/

model based control focuses [13]. However, the power capacity of this model is small which is built based on a 160 MW unit in Sweden. Recently, a dynamic model of supercritical once-through boiler units is developed based on the law of conservation of energy and substance, and some necessary assumptions [14]. This dynamic model with three inputs and three outputs is developed for controller design and dynamic analysis. To develop a model that is suitable for the direct energy balance (DEB) coordinated control scheme, a dynamic model is proposed to describe each module by yielding a 6th-order nonlinear model [15]. The accuracy is verified by the field measurements from a 300 MW coal-fired plant. Considering that the DEB control scheme (it will be introduced in subsection 4.1), which is widely used by field engineers in thermal power plants, the analysis and verification of the proposed gain scheduling design based on active disturbance rejection control (ADRC) are carried out based on this model.

To relieve the adverse effects of the nonlinearity and strong coupling of power plants, and obtain the faster power output and smaller pressure fluctuation, many control strategies are proposed to solve the aforementioned control difficulties. Model predictive control (MPC), with distinct advantages in explicitly handling constraints and multivariable couplings, has been applied to the coordinated control system (CCS) which is the most important and crucial loop in any thermal power plant [16,17]. Nonlinear MPC and economic MPC based on nonlinear models are designed and discussed for boiler-turbine systems, respectively. Nonlinear control based on feedback linearization approach is proposed to enhance the disturbance rejection ability and power-tracking rate [18,19]. An optimized nonlinear controller using evolutionary algorithms is designed for boiler-turbine system in Ref. [20]. Besides, sliding mode control [21,22], H_∞ robust control [23], dynamic matrix control [24], self-adaptive PID control [25] and neural network inverse control [26] are also researched to improve the control performance of thermal power plants. These control strategies all show satisfactory control effect in numerical simulations while these aforementioned control strategies were rarely used in practical units due to the following reasons [27]:

1) These control strategies could obtain satisfactory control effect at the cost of a large computation complexity which results great implementation difficulty in the distributed control system (DCS) platform.
2) Besides, the accurate mathematical model is the foundation for some model-based control strategies while the accurate model is hard or expensive to build because of the system complexity.

In the past decades, ADRC gradually develops into a powerful tool to handle the control difficulties caused by unknown dynamics and external disturbances [28,29]. It offers a new perspective where unmeasured disturbances and un-modeled dynamics can be estimated and compensated in real time by an extended state observer (ESO) [30]. Moreover, it is independent of the accurate mathematical model and can be implemented in the DCS easily. The convergence of the tracking differentiator and the stability of ESO are discussed in Refs. [31,32], respectively. Based on the theoretical analysis and distinct advantages of ADRC, ADRC has been successfully applied to motion system [33], engines system [34], fan system in server [35], organic Rankine cycle (ORC) system [36] and secondary air system [2] et al. These systems with ADRC have better tracking performance and stronger disturbance rejection ability than that of other comparative control strategies based on their own experiment platforms. However, the control performance under wide operating conditions is not verified in these experiments.

Recently, ADRC is also proposed for the CCS to solve the control difficulties such as the coupling, nonlinearity, et, al. In Ref. [37], the control strategy based on ADRC is designed for a power plant with a single loop, where a tracking differentiator, an ESO and a nonlinear combination of errors are combined to improve the control performance. ADRC based on the DEB control scheme is designed for the CCS to reduce the pressure fluctuation [38]. However, the ability of the ADRC is still limited by faster response speed responding to the AGC command. The faster response speed can result in challenges of the equipment safety. What is worse, thermal power plants have to enlarge their operating conditions to absorb more renewable power into the power grid. Now thermal power plants shift the power output in the range of [50%, 100%] of full load. Thermal power plants will have a larger range of [30%, 100%] of full load to absorb more renewable power into the power grid in the future. This can result in stronger nonlinearity of the unit and greater safety pressure. To solve this, a mature method namely gain scheduling can be applied to speed up load responses and reduce pressure fluctuations. The whole operating condition can be divided into several typical conditions and controllers are designed for each condition with the switching law for the design of gain scheduling [39]. The gain scheduling designs combining with adaptive fuzzy PID control [40], iterative learning control [41], sliding mode control [42] and MPC [43] have been studied for different systems. These control strategies still have a large computation complexity which limits the practical application of the gain scheduling.

To deal with control difficulties of thermal power plants and reduce the implementation difficulties of gain scheduling, a gain scheduling design based on ADRC is proposed for thermal power plants under full operating conditions from 30% to 100% of full load. Besides, to the best of authors' knowledge, there are few references to discuss the gain scheduling design based on ADRC, such as the switching method of ADRC parameters and stability analysis for the gain scheduling design based on ADRC. Besides, the following interesting outcomes, as the main achievements, are briefly summarized:

1) A gain scheduling design based on ADRC is proposed for thermal power plants under full operating conditions.
2) The selection of the scheduling parameter is discussed, and a simple yet effective linear switching method for the observer bandwidth ω_o and controller bandwidth ω_c is proposed.
3) The stability analysis of the proposed control strategy based on the Kharitonov theorem is discussed qualitatively and the quantitative calculation of the stability regions for ADRC parameters is carried out.
4) The superiority of the proposed control strategy compared to the regular ADRC and the PI is verified by simulations with different load tracking rates and disturbance rejection with the coal quality variation under different operating conditions.

The rest of the paper is organized as follows: a dynamic model of CCS and control objectives are introduced briefly, and the CCS control difficulties are discussed to explain the necessity of the proposed control strategy in Section 2. Section 3 provides the brief principle of ADRC, the tuning method and stability region of ADRC parameters. In Section 4, the necessary analysis of the gain scheduling design based on ADRC are discussed such as the selection of the scheduling parameter, the switching method for ω_o and ω_c, and stability analysis for the gain scheduling design based on ADRC. The superiority of the proposed strategy compared to the regular ADRC and the PI is verified by simulations in Section 5. Conclusions are drawn in Section 6.

2. Problem formulation

2.1. Dynamic model of coordinated control system

In this paper, the gain scheduling design based on ADRC is discussed for the nonlinear dynamic model in Ref. [15] considering that the model is suitable for the DEB control scheme which is widely used by field engineers in thermal power plants.

This model contains six parts and the description is shown as follows:

Dynamic of the flow of coal blowing into the furnace,

$$\dot{q}_f = \frac{1}{22}\left[u_B(t-43) - q_f\right], \tag{1}$$

Dynamic of the steam evaporation amount,

$$\dot{D}_b = \frac{1}{380}\left[2.46k_c q_f^{1.230} - D_b\right], \tag{2}$$

Dynamic of the boiler pressure,

$$\dot{p}_b = \frac{1}{4057}\left[D_b - 42.51p_b^{0.956}\sqrt{p_b - p_T}\right], \tag{3}$$

Dynamic of the throttle pressure,

$$\dot{p}_T = \frac{1}{5101}\left[42.51p_b^{0.956}\sqrt{p_b - p_T} - D_T\right], \tag{4}$$

Dynamic of the governing stage pressure,

$$\dot{p}_1 = \frac{1}{5}[0.0083\mu_t p_T - p_1], \tag{5}$$

Dynamic of the inlet steam mass flow,

$$\dot{D}_T = \frac{1}{5}[74.74p_1 - D_T], \tag{6}$$

where u_B (t/h) and μ_t (%) are the coal feed and the throttle opening position, respectively.

Besides, the power output N_e can be calculated by

$$N_e = 0.86D_T^{0.852}, \tag{7}$$

Moreover, the normalization coefficient k_c in Equation (2) is introduced to represent the influence of the coal quality, which should equal to 100% under the normal condition. Besides, considering the protection of actuators of the boiler and turbine, and the operation rules of boiler and turbine, we can obtain the amplitude limit and rate limit as follows,

$$\begin{aligned} &0 \le u_B \le 150, \\ &-0.3 \le \dot{u}_B \le 0.3, \\ &0 \le \mu_t \le 100, \\ &-0.2 \le \dot{\mu}_t \le 0.2, \end{aligned} \tag{8}$$

Note that the rate limit listed in Equation (8) is different from that in Ref. [15], where $\dot{u}_B$ and $\dot{\mu}_t$ are both ±0.1. The rate limit in Ref. [15] is conservative with the development of material technology and improvement of equipment operation level.

In this model, the coal feed u_B and throttle opening position μ_t are the control inputs. The process outputs are the power output N_e (MW) and throttle pressure p_T (MPa), respectively. Hereby a standard nonlinear model for control can be derived from Equations (1)–(6) as,

$$\begin{cases} \dot{\boldsymbol{x}} = f(\boldsymbol{x}, \boldsymbol{u}) \\ \boldsymbol{y} = h(\boldsymbol{x}) \end{cases}, \tag{9}$$

where $\boldsymbol{u} = [u_B \ \mu_t]^T$, $\boldsymbol{x} = [q_f \ D_b \ p_b \ p_T \ p_1 \ D_T]^T$ and $\boldsymbol{y} = [Ne \ p_T]^T$.

To better rule in peak-load shaving and play a greater potential, the excepted operating range would be expanded to [30%–100%] of the full load. Note that the constant and sliding pressure operation modes both exist in the actual thermal power plant to improve energy efficiency and meet safety requirements. Specifically, the thermal power plant would be on the constant pressure operation mode when the output power locates in the ranges of 30%–40% and 90%–100% to improve energy efficiency and ensure the system security, respectively. In other ranges, the thermal power plant would operate on the sliding pressure operation mode.

Moreover, some typical operating conditions are calculated and listed in Table 1 based on the dynamic model in Equations (1)–(6).

Generally, the CCS has some fundamental control requirements to respond the AGC command quickly and satisfy the safety and economic requirements, which are listed as follows [45]:

1) The power output should be adjusted timely as required by the AGC command. In China, the tracking rate is about 1.5 %–2% of full load per minute, which means that it requires to generate 4.5–6 MW more power in 1 min for a 300 MW thermal power plant.
2) The reverse change of the throttle pressure when regulating the power output should be limited to a safety bound on the sliding pressure operation mode, e.g., ±0.4 MPa from the initial pressure. Besides, the biggest deviation also should be limited to a safe bound on the constant pressure operation mode, e.g., ±0.4 MPa from the initial pressure. Note that the system requires a manual intervention when the deviation is bigger than ±0.4 MPa to ensure the system security. The fewer manual interventions, the better control performance for thermal power plants.

2.2. Control difficulties

The CCS of thermal power plants has many difficulties such as the strong nonlinearity, strong coupling and the wide change of operating conditions. These control difficulties are analyzed in this subsection.

Firstly, the Vinnicombe gap metric is used to measure the system nonlinearity of the model in Equations (1)–(7) or Equation (9). The definition and calculation of the Vinnicombe gap matric can be seen in Ref. [44]. Note that the closer value (ν_g) to one, the stronger nonlinearity of the system, and vice versa. The nominal condition is chosen as the full load, E (100%) shown in Table 1, where $N_e = 300.1$ MW and $p_T = 16.09$ MPa, and the nominal transfer matrix model can be obtained by the model linearization. The distance measure between the nominal model and other models

Table 1
Fiver typical operating conditions.

Operating condition	N_e (MW)	p_T(MPa)	u_B (t/h)	μ_t (%)
A (30%)	90.0	13.82	40.7	27.4
B (40%)	120.6	13.82	53.8	38.6
C (65%)	195.3	14.81	85.2	63.4
D (90%)	270.0	16.09	116.1	85.4
E (100%)	300.1	16.09	128.4	96.7

that are linearized with different N_e and p_T is depicted in Fig. 1.

Obviously, a large v_g exists when N_e and p_T are far from the nominal model which means that a strong nonlinearity exists for the model in Equations (1)–(7) or Equation (9). Besides, an obvious valley in the 3-D figure of distance measure can be seen in Fig. 1, showing that least amount of nonlinearity. This indicates that the nonlinearity can be somewhat avoided if the set-points of N_e and p_T are changing in proportion along the valley line. This valley is fully used to reduce the nonlinearity of the system in engineering practice called sliding pressure operation mode. Note that the sliding pressure operation mode is not always reasonable in some operating conditions and is not applicable when the output power is very small or large because of the economical and safe considerations.

Besides, the linearized models under typical operating conditions in Table 1 can be obtained by the linearization method and their open-loop responses are presented in Fig. 2. The dynamic characteristics of the CCS vary greatly due to the wide operating conditions, especially the dynamic characteristics of the pressure loop as shown in Fig. 2 (c) and (d). Besides, the strong coupling is also seen in Fig. 2 because each control input has obvious influence on both outputs.

3. Active disturbance rejection control

The ADRC gets more and more attention and successful applications, and stands out among control algorithms owing to the following merits:

(I) The ADRC is largely independent of precise mathematical models which are hard or expensive to obtain for industrial process because of the system complexity.
(II) The robustness of the ADRC is stronger than the conventional PI/PID controller and can ensure good control performance when the system is far from the nominal condition.
(III) The control law of the ADRC is simple, consisting of some basic algebraic computation, and can be easily implemented via existing function blocks in the DCS platform.
(IV) The ADRC is conceived from the perspective of disturbance rejection, which can balance the tradeoff relationship between tracking and disturbance rejection well, especially for the CCS whose two loops both have the tasks of the tracking and disturbance rejection.

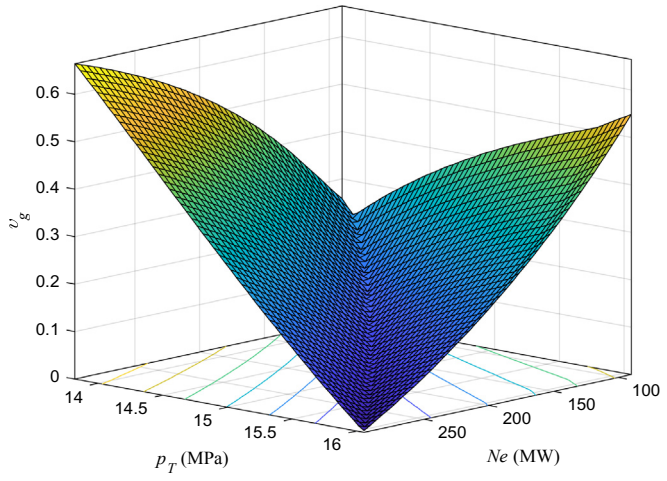

Fig. 1. Distance measure from the nominal model linearized at (300.1 MW, 16.09 MPa) to the models linearized with different N_e and p_T.

In this section, the principle of the first order ADRC is briefly introduced. Besides, the parameter tuning and stability region of the ADRC are also discussed.

3.1. Brief principle of ADRC

To reduce the difficulty of implementation, the first order and second order ADRC controllers are the most widely used ADRCs in practice despite the order mismatch between the system order and the ADRC order. Moreover, the capacity of the low-order ADRC to control high-order systems has been theoretically proved [46] and verified in superheated steam temperature system [47] and fractional-order system [48].

In this paper, the first order ADRC is discussed and its structure is illustrated in Fig. 3. r, y, d and u are the reference input, the system output, the external disturbance and the control signal, respectively. z_2 is the output of the ESO. Besides, k_p and b_0 are the parameters of the control law.

Generally, a system can be arranged into a first order form depicted by

$$\dot{y} = g(t, y, \ddot{y}, \cdots, d, \omega) + bu, \tag{10}$$

where g is the synthesis function of time-variant (t), high-order ($\ddot{y}$), external disturbance (d), dynamic uncertainties (ω), etc. in the system, and b is the input gain whose value may be unknown for the plant.

Define $f = g + (b - b_0)u$, where b_0 is the estimation of input gain b. Then Equation (10) can be transformed into,

$$\dot{y} = f + b_0 u, \tag{11}$$

where f is called the total disturbance which includes the external disturbances and the unknown internal dynamics of the system [28]. Denote $y = x_1$ and let f be an extended state x_2, the state space representation of Equation (11) can be depicted as,

$$\begin{cases} \begin{bmatrix} \dot{x}_1 \\ \dot{x}_2 \end{bmatrix} = \begin{bmatrix} 0 & 1 \\ 0 & 0 \end{bmatrix} \begin{bmatrix} x_1 \\ x_2 \end{bmatrix} + \begin{bmatrix} b_0 \\ 0 \end{bmatrix} u + \begin{bmatrix} 0 \\ 1 \end{bmatrix} \dot{f} \\ y = \begin{bmatrix} 1 & 0 \end{bmatrix} \begin{bmatrix} x_1 \\ x_2 \end{bmatrix} \end{cases}, \tag{12}$$

Then the ESO is designed for the system in Equation (12) as,

$$\begin{bmatrix} \dot{z}_1 \\ \dot{z}_2 \end{bmatrix} = \begin{bmatrix} -\beta_1 & 1 \\ -\beta_2 & 0 \end{bmatrix} \begin{bmatrix} z_1 \\ z_2 \end{bmatrix} + \begin{bmatrix} b_0 & \beta_1 \\ 0 & \beta_1 \end{bmatrix} \begin{bmatrix} u \\ y \end{bmatrix}, \tag{13}$$

where z_2 can track f well when β_1 and β_2 are tuned appropriately. The estimated total disturbance can be compensated in real time,

$$u = \frac{u_0 - z_2}{b_0}, \tag{14}$$

The plant after the compensation is depicted as,

$$\dot{y} = f + b_0 \frac{u_0 - z_2}{b_0} \approx f + \frac{u_0 - f}{b_0} = u_0, \tag{15}$$

Therefore, the controlled plant becomes an integral process and a control law shown in Fig. 3 is depicted by

$$u_0 = k_p(r - y), \tag{16}$$

which is a proportional controller. The desirable closed-loop

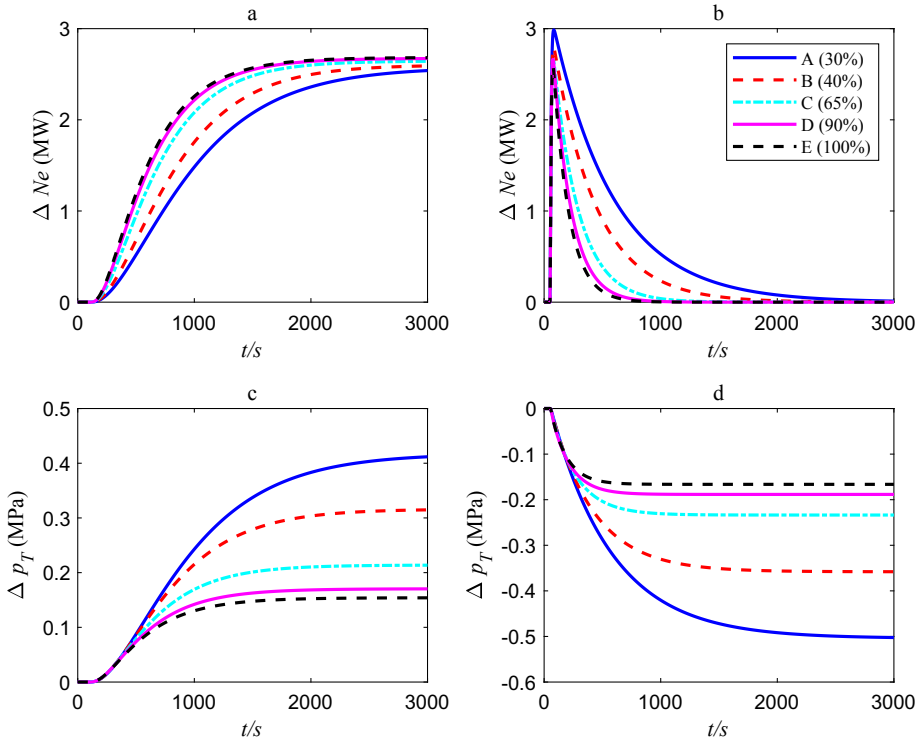

Fig. 2. Open-loop responses under five typical operating conditions. ((a) and (c): the step of u_B; (b) and (d): the step of μ_t).

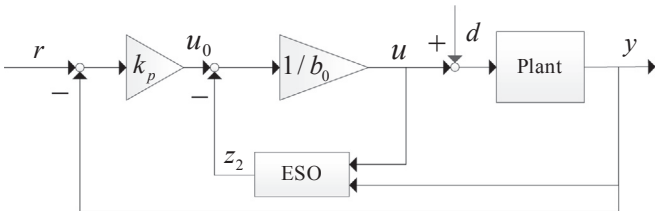

Fig. 3. The structure of the first order ADRC.

transfer function can be obtained based on Equation (15) and Equation (16) as,

$$G_{lc}(s) = \frac{y(s)}{r(s)} = \frac{k_p}{s + k_p}, \tag{17}$$

Note that k_p has the practical physical meaning, namely the controller bandwidth. Moreover, β_1 and β_2 can be tuned by the bandwidth-parameterization method proposed in Ref. [49],

$$\begin{cases} \beta_1 = 2\omega_o \\ \beta_2 = \omega_o^2 \end{cases}, \tag{18}$$

where ω_o is named the observer bandwidth.

3.2. Tuning method and stability region of the ADRC

Based on the introduction of the ADRC in subsection 3.1, we can know that there are three parameters the observer bandwidth ω_o, the controller bandwidth k_p and b_0 to be tuned. The following rules may serve as a guidance to tune the parameters:

(I) A large k_p or a small b_0 leads to a quick response which in turn requires increased control force while the stability margin would be small. Besides, the response would have a large overshoot and the fluctuation would increase due to the strong control intervention with a too large k_p or a too small b_0. Note that the value of b_0 should meet $b/b_0 \in (0,\ 2)$ to ensure the stability and convergence of the ESO [50].

(II) The ability of the observation and the compensation of the total disturbance would increase with the increased ω_o, and so does noise sensitivity of the ESO. Therefore, ω_o should be gradually augmented to a proper value which could ensure a good estimation of the ESO.

Based on the discussion of the influence of parameters on control performance, a tuning procedure can be summarized as follows:

1) b_0 should be selected firstly, and the value of b_0 should meet $b/b_0 \in (0,\ 2)$ to ensure the stability and convergence of the ESO. A large b_0 is recommended to avoid the non-convergence when the real gain b is not exactly known.
2) Then k_p can be selected based on the desired closed-loop dynamic as shown in Equation (17) and ω_o can be gradually augmented to a proper value to enhance the observation ability of the ESO.
3) If the ADRC with these parameters can obtain the satisfactory control performance, the tuning procedure can stop. Otherwise, repeat the step 1)-2) again.

The flow chart is accordingly given in Fig. 4 to guide the tuning in engineering practice. Note that the bandwidth-parameterization method works well and the presented tuning procedure involves trial and error tests.

The first order ADRC can be can be transformed into an equivalent two-degrees-of-freedom (TDOF) control structure as shown

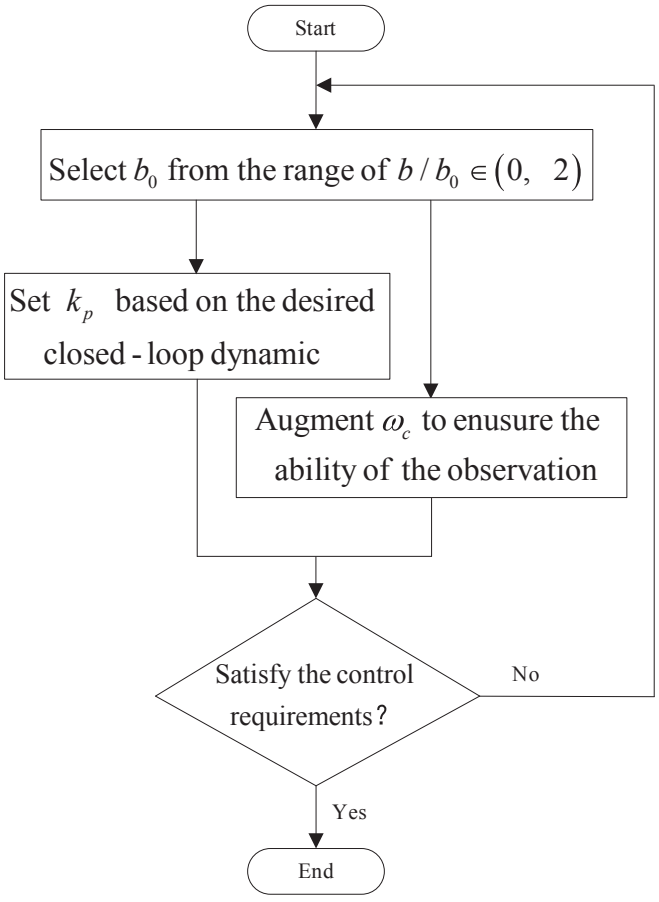

Fig. 4. Flow chart of the ADRC parameters tuning.

in Fig. 5 [51], where the feedback controller and feedforward controller are depicted by

$$G_c(s) = \frac{k_p s^2 + (\omega_o^2 + 2k_p\omega_o)s + k_p\omega_o^2}{(s + 2\omega_o)b_0 s}, \tag{19}$$

and

$$G_f(s) = \frac{k_p(s + \omega_o)^2}{k_p s^2 + (2k_p\omega_o + \omega_o^2)s + k_p\omega_o^2}, \tag{20}$$

To simplify the stability region analysis of the ADRC, the plant transfer function can be depicted by

$$G_p(i\omega) = r(\omega)e^{i\vartheta(\omega)} = a(\omega) + ib(\omega), \tag{21}$$

The characteristic equation for the closed-loop system is represented as,

$$1 + G_l(s) = 0, \tag{22}$$

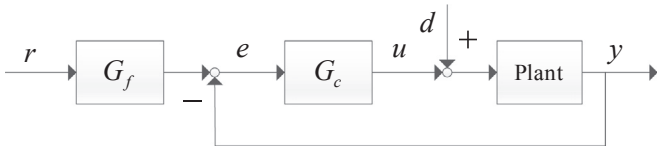

Fig. 5. Equivalent structure of ADRC.

where $G_l(s) = G_p(s)G_c(s)$ is called the loop transfer function.

By substituting Equations (19) and (21) into Equation (22) and separating the real and imaginary parts, we can obtain,

$$\begin{cases} k_p\left(\omega_o^2 - \omega^2\right)a(\omega) - \left(\omega_o^2 + 2k_p\omega_o\right)b(\omega)\omega - b_0\omega^2 = 0 \\ k_p\left(\omega_o^2 - \omega^2\right)b(\omega) + \left(\omega_o^2 + 2k_p\omega_o\right)a(\omega)\omega + 2b_0\omega_o\omega = 0 \end{cases}, \tag{23}$$

By solving Equation (23) with the fixed b_0, we can obtain the boundary of stability region. Considering that k_p and ω_o should be greater than zero to ensure the system stability, these boundaries form the stability region of the ADRC.

Now the procedure of the stability region calculation is summarized as follows:

1) The plant in Equation (21) is known and b_0 should be fixed firstly according to the discussion above.
2) The boundary of the ADRC can be calculated by solving the expression in Equation (23) with ω varies from zero to $+\infty$. Note that upper value of ω can be set a sufficiently large value. We can obtain the stability region of the ADRC with the fixed b_0.
3) The whole stability regions of the ADRC can be obtained by repeating the calculation for a set of b_0 -values.

Consider a first order plus dead time (FOPDT) plant depicted by

$$G_p(s) = \frac{1.2}{4s + 1}e^{-1.5s}, \tag{24}$$

whose real gain b is 0.3. By applying the calculation procedure discussed above, we can obtain the stability regions of the ADRC with gridded b_0 from 0.15 to 5 as shown in Fig. 6. We can know that a larger b_0 means a larger parameter selection region, and this explains the reason why a large b_0 is recommended. The discussion about the stability region of the ADRC offers a parameter selection region and a foundation of the asymptotic stabilization analysis for the smooth switching.

4. Gain scheduling design based on ADRC

In this section, the principle of the DEB is introduced firstly to understand the control structure which is a widely-used structure in thermal power plants, especially in giant-scale thermal power plants. Then some necessary discussions of the division of

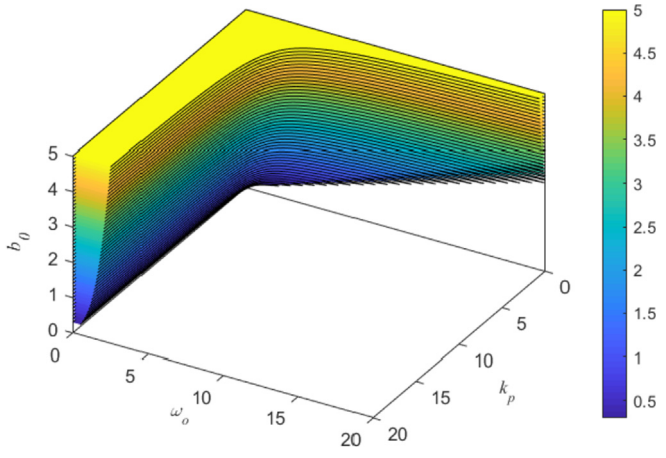

Fig. 6. The stability regions of ADRC with gridded b_0.

operating conditions and the selection of scheduling parameters are presented. A linear switching method is developed based on the foundations discussed above. In the end, the stability analysis based the Kharitonov theorem and the quantitative calculation are carried out to offer the stability regions which can ensure the asymptotic stabilization of the closed-loop system under full operating conditions.

4.1. Brief principle of the DEB

The control structure of the DEB is shown in the red dashed box of Fig. 7, where the controlled variable of the throttle pressure loop is the energy heat signal depicted by

$$Q_m = p_1 + C_b \frac{dp_b}{dt}, \tag{25}$$

which replaces the throttle pressure p_T and $C_b = 120$. Correspondingly, the set-point of the throttle pressure loop becomes the energy demanding signal,

$$r_{Q_m} = r_{p_t} \frac{p_1}{p_T}, \tag{26}$$

where r_{p_t} is the set-point of p_T and it comes from the AGC command by a lookup table.

When the system is at steady state, we have $Q_m = r_{Q_m}$ and $dp_b/dt = 0$, and we have the following equation,

$$p_1 = p_r \frac{p_1}{p_T}, \tag{27}$$

which means the throttle pressure p_T can converge to its set-point p_r when the system is at steady state. The advantage of the DEB control structure is that it can reduce the coupling effect from the throttle pressure loop to the power output greatly [37].

Based on the control structure of the DEB, the output of throttle pressure loop becomes the energy heat signal Q_m which replaces the throttle pressure p_T and the linearized model can be depicted by

$$\begin{bmatrix} N_e \\ Q_m \end{bmatrix} = \begin{bmatrix} g_{11}(s) & g_{12}(s) \\ g_{21}(s) & g_{22}(s) \end{bmatrix} \begin{bmatrix} u_B \\ \mu_t \end{bmatrix}, \tag{28}$$

Similarly, $\boldsymbol{y}$ in Equation (9) changes to $\boldsymbol{y} = [Ne \;\; Q_m]^T$ and Q_m can be calculated by

$$Q_m = p_1 + \frac{C_b}{4057}\left[D_b - 42.51 p_b^{0.956}\sqrt{p_b - p_T}\right], \tag{29}$$

Note that the throttle opening position μ_t is selected to control the power output Ne because that this benefits the quick tracking of the AGC command which is the first priority for any thermal power plant. Correspondingly, the coal feed u_B is selected to control the energy heat signal. To accelerate the response of throttle pressure loop, a feedforward PD controller $G_f(s)$ which is from the load demand is added to the coal feed u_B. $G_{N_e\_c}(s)$ and $G_{p_T\_c}(s)$ are the feedback controllers of the power output loop and throttle pressure loop, respectively.

4.2. Division of operating conditions and selection of scheduling parameter

Firstly, we discuss the division of operating conditions for CCS which is the foundation of gain scheduling design. The following factors should be considered,

(I) The more scheduling ranges means the more meticulous control which can ensure the better control performance.
(II) The adverse influence of more scheduling ranges should not be neglected, such as the exponentially increased design workload and the implementation difficulty in DCS platform.

Therefore, the number of scheduling ranges is a tradeoff between the control performance and the cost of design and implementation. The scheduling ranges in this paper are selected as shown in Fig. 8. The scheduling ranges are from F to G and from H to I, respectively. Besides, the steady state parameters of the selected operating conditions are listed in Table 2 and the scheduling range is about 10 MW. To a great extent, this tradeoff can reduce the design working load and the implementation difficulty, and balance the control requirements of different dynamic characteristics.

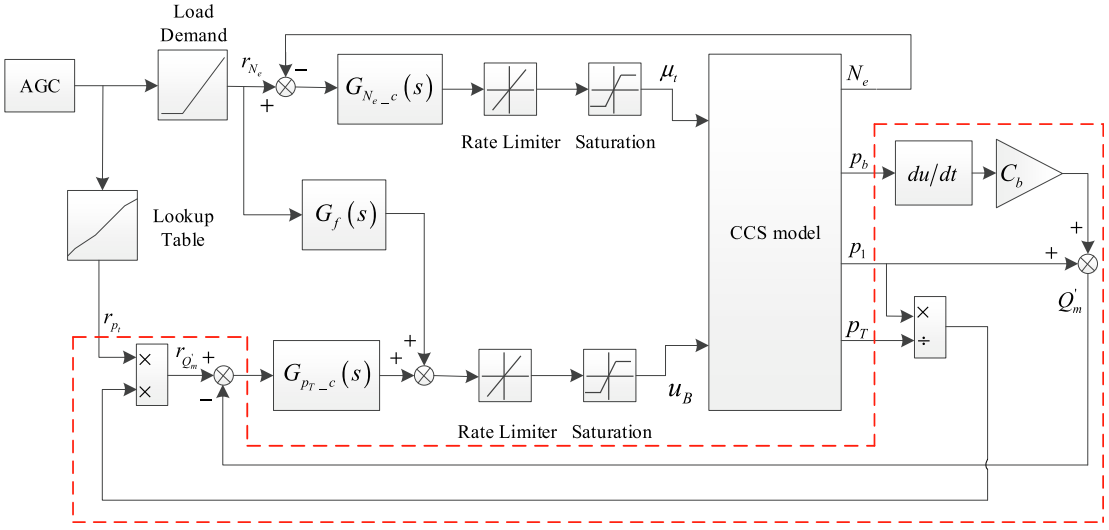

Fig. 7. The DEB control structure for CCS system with actuator constraints.

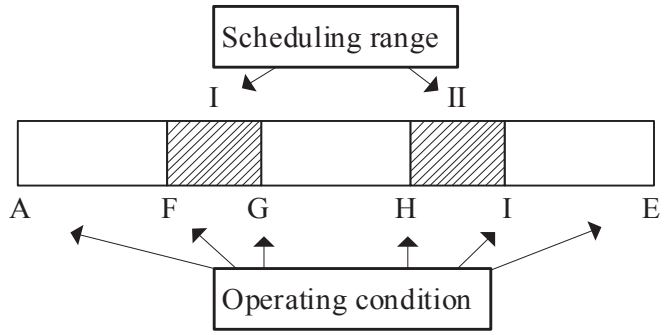

Fig. 8. The scheduling ranges and the operation conditions selected under full operating conditions.

Table 2
The operating conditions for the gain scheduling design.

Operating condition	N_e (MW)	p_T(MPa)	u_B (t/h)	μ_t (%)
A (30%)	90.0	13.82	40.7	27.4
F (50%)	150.1	14.31	66.3	48.2
G (56.7%)	169.9	14.58	74.6	54.7
H (73.3%)	219.8	15.33	95.4	70.4
I (80%)	240.1	15.63	103.8	76.6
E (100%)	300.1	16.09	128.4	96.7

Besides, the load demand is selected as the scheduling parameter owing to the following reasons:

(I) The load is a controlled variable and it is measurable.
(II) The load is a key parameter for the CCS and the change of dynamic characteristics depends on the load change largely. Its variation naturally represents various operating points of the CCS, especially when the power plant is operating under the constant pressure operation mode.
(III) The most important factor is that all coefficients of linearized models are monotonous with the monotonous change of load. Take $g_{12}(s)$ in Equation (28) as an example, and denote the coefficients of the numerators and denominators as $\boldsymbol{n} = [n_2\ \ n_1]$ and $\boldsymbol{d} = [d_4\ \ d_3\ \ d_2\ \ d_1]$, respectively. We can obtain the monotonous trends of them under the different operating conditions shown in Fig. 9. Note that other coefficients in Equation (28) all have the monotonous trends with the monotonous change of load.

Finally, the ADRC parameters, which should be changed to response to the scheduling parameter, need to be discussed. Although the ADRC has three parameters the observer bandwidth ω_o, the controller bandwidth k_p and the estimated input gain b_0, the parameters involved the gain scheduling design are selected as ω_o and k_p except b_0. The reasons of this decision are described qualitatively as follows:

(I) As the discussion in subsection 3.2, a larger k_p means a stronger control force and the changing k_p can adjust the dynamic characteristics of closed-loop system reasonably. Besides, ω_o can reflect the observation and compensation ability of the total disturbance so a changing ω_o in the gain scheduling design is also necessary.
(II) b_0 is the estimation of the real input gain b and the b_0 is often larger than the real value. The changing b_0 would result a large overshoot because that b_0 is the denominator of Equation (14) whose output is the control signal.

4.3. Gain scheduling design based on ADRC under full operating conditions

To simplify the analysis, consider a first order system with uncertain parameters,

$$G(s) = \frac{\alpha_1(\theta)}{\lambda_1(\theta)s + 1}, \tag{30}$$

where $\alpha_1(\theta)$ and $\lambda_1(\theta)$ are both bounded real numbers and their scopes can be obtained according to the operating conditions of the system. θ is the scheduling parameter as discussed in subsection 4.2. The division of operating conditions can be rearranged as shown in Fig. 10 based on Fig. 8. The division of operating conditions is a continuous range as shown in Fig. 10 and the two adjacent operating ranges have a small overlap range which is the scheduling range as shown the hatched section in Fig. 10. For example, the range $[\theta_{i+1}\ \theta_{i+1+\Delta}]$ is the overlap range between the operating range $[\theta_i\ \theta_{i+1+\Delta}]$ and the operating range $[\theta_{i+1}\ \theta_{i+2+\Delta}]$.

For each operating ranges, we can calculate the intervals of all coefficients in Equation (30). The intervals for the operating range $[\theta_i\ \theta_{i+1+\Delta}]$ can be obtained that $\alpha_1 \in [\alpha_{1\min}\ \alpha_{1\max}]$ and $\lambda_1 \in [\lambda_{1\min}\ \lambda_{1\max}]$, and we can obtain the function family in the operating range $[\theta_i\ \theta_{i+1+\Delta}]$,

$$G(s) = \frac{\alpha_1}{\lambda_1 s + 1}, \tag{31}$$

where $\alpha_1 \in [\alpha_{1\min}\ \alpha_{1\max}]$ and $\lambda_1 \in [\lambda_{1\min}\ \lambda_{1\max}]$.

Design the ADRC controller $\{k_{p\_i},\ \omega_{o\_i},\ b_0\}$ for the operating range $[\theta_i\ \theta_{i+1+\Delta}]$ and the ADRC controller $\{k_{p\_i+1},\ \omega_{o\_i+1},\ b_0\}$ for the operating range $[\theta_{i+1}\ \theta_{i+2+\Delta}]$. Note that these two ADRC controllers both ensure the stability for the system in the range $[\theta_{i+1}\ \theta_{i+1+\Delta}]$ and b_0 is fixed as discussed in subsection 4.2. Based on the feedback controller $G_c(s)$ in Equation (19) and the controlled plant in Equation (31), the eigenpolynomial can be depicted as $T_i(s)$ and $T_{i+1}(s)$ whose specific expressions can be seen Equations (A-1) - (A-2) in Appendix A. Therefore, we have inequalities (A-3) - (A-10) listed in Appendix A by applying the Routh stability criterion.

For the scheduling range $[\theta_{i+1}\ \theta_{i+1+\Delta}]$, we design the ADRC controller based on the gain scheduling and the ESO is depicted by

$$\begin{bmatrix} \dot{z}_1 \\ \dot{z}_2 \end{bmatrix} = \begin{bmatrix} -2\left[\phi\omega_{o\_i} + (1-\phi)\omega_{o\_i+1}\right] & 1 \\ -\left[\phi\omega_{o\_i} + (1-\phi)\omega_{o\_i+1}\right]^2 & 0 \end{bmatrix} \begin{bmatrix} z_1 \\ z_2 \end{bmatrix} + \begin{bmatrix} b_0 & \left[\phi\omega_{o\_i} + (1-\phi)\omega_{o\_i+1}\right] \\ 0 & \left[\phi\omega_{o\_i} + (1-\phi)\omega_{o\_i+1}\right] \end{bmatrix} \begin{bmatrix} u \\ y \end{bmatrix}, \tag{32}$$

The control law is depicted by

$$u_0 = \left[\phi k_{p\_i} + (1-\phi)k_{p\_i+1}\right](r - y), \tag{33}$$

Based on the TDOF control structure of the ADRC in subsection 3.1, the feedback controller can be depicted as $G_{c*}(s)$ whose specific expression can be seen Equation (A-11) and we have $\phi \in [0, 1]$. Based on the feedback controller $G_{c*}(s)$ and the system in Equation (31), we can obtain the eigenpolynomial $T_{i*}(s)$ depicted as Equation (A-12) in Appendix A. By the transformation of inequalities (A-3) - (A-10), we can obtain the inequality (A-13), which means that the controller in Equation (A-11) can ensure the convergence of the closed-loop system.

Therefore, we have the scheduling method of ADRC parameters for the scheduling range $[\theta_{i+1}\ \theta_{i+1+\Delta}]$,

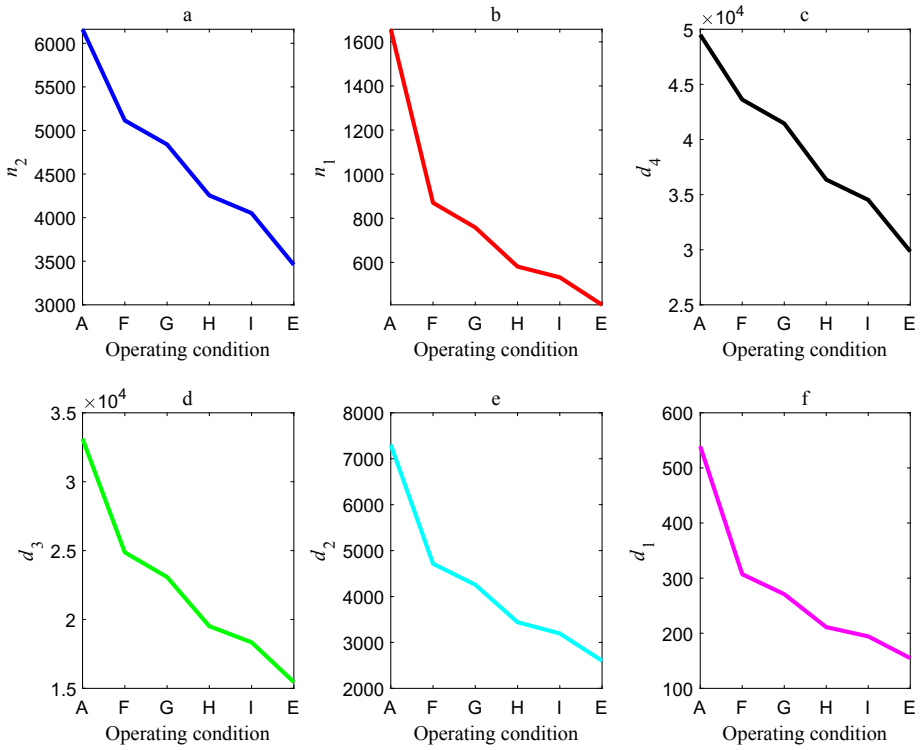

Fig. 9. The trends of coefficients in $g_{12}(s)$ with the load change.

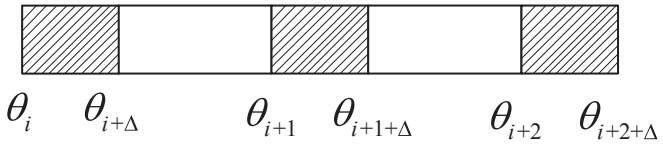

Fig. 10. The rearranged diagram of the scheduling ranges.

$$k_p = \begin{cases} k_{p\_i}, & \theta \in (\theta_{i+\Delta}, \theta_{i+1}) \\ \dfrac{\theta_{i+1+\Delta} - \theta}{\theta_{i+1+\Delta} - \theta_{i+1}} k_{p\_i} + \dfrac{\theta - \theta_{i+1}}{\theta_{i+1+\Delta} - \theta_{i+1}} k_{p\_i+1}, & \theta \in [\theta_{i+1}, \theta_{i+1+\Delta}] \\ k_{p\_i+1}, & \theta \in (\theta_{i+1+\Delta}, \theta_{i+2}) \end{cases} \tag{34}$$

and

$$\omega_o = \begin{cases} \omega_{o\_i}, & \theta \in (\theta_{i+\Delta}, \theta_{i+1}) \\ \dfrac{\theta_{i+1+\Delta} - \theta}{\theta_{i+1+\Delta} - \theta_{i+1}} \omega_{o\_i} + \dfrac{\theta - \theta_{i+1}}{\theta_{i+1+\Delta} - \theta_{i+1}} \omega_{o\_i+1}, & \theta \in [\theta_{i+1}, \theta_{i+1+\Delta}] \\ \omega_{o\_i+1}, & \theta \in (\theta_{i+1+\Delta}, \theta_{i+2}) \end{cases} \tag{35}$$

Note that the analysis about the scheduling method is based on a first order system, when the controlled plant is a plant with time delay, the analysis difficulty will increase exponentially. Fortunately, considering controlled plant in Equation (28) can be approximated as a first order plus time delay (FOPTD) system depicted by

$$G_{eq}(s) = \frac{k}{Ts + 1} e^{-Ls}, \tag{36}$$

The equivalent plant is a lag-dominant process considering $L/(T + L)$ is about 0.15 ($\pm$0.05) under all operating conditions and the influence of the time delay is weak and can be dealt with a first order system. Therefore, we can conclude that the proposed gain scheduling method works well for the system in Equation (28) roughly. Besides, the effectiveness of the scheduling method for Equation (28) can be verified in Section 5. The scheduling method can ensure the stability of the closed-loop system when the system changes slowly [52].

4.4. The stability analysis based on the Kharitonov theorem

In this subsection, the qualitative stability analysis based on the Kharitonov theorem is discussed and then the quantitative calculation of the stability regions of ADRC parameters is carried out to provide the parameter regions. The stability analysis based on the Kharitonov theorem offers us a theoretical method to analyze the stabilizability of the proposed gain scheduling design based on ADRC for the interval systems.

The Kharitonov theorem offers the sufficient condition for the judgement whether the ADRC controller can stabilize the entire interval function family [53]. Take $g'_{22}(s)$ in Equation (28) as an example, and $g'_{22}(s)$ can be rearranged with uncertain parameters as,

$$g'_{22}(s) = \frac{n_3 s^3 + n_2 s^2 + n_1 s + n_0}{d_4 s^4 + d_3 s^3 + d_2 s^2 + d_1 s + 1}, \tag{37}$$

where $n_i \in [n_{i\min}\ n_{i\max}]$ $(i = 0, 1, 2, 3)$ and $d_j \in [d_{j\min}\ d_{j\max}]$ $(j = 1, 2, 3, 4)$.

Based on the feedback controller $G_c(s)$ in Equation (19) and the

controlled plant in Equation (37), we can obtain the eigenpolynomial $T(s)$ depicted as Equation (B-1) in Appendix B.

We can obtain the corresponding four Kharitonov functions (Equations (B-2) - (B-5) in Appendix B, where the expressions of A_{0_min}, A_{0_max} et al. in Kharitonov functions are listed in Appendix B.

If ADRC parameters can ensure that all Kharitonov functions in Equations (B-2) - (B-5) are Hurwitz, we can say that these ADRC parameters $\{k_p,\ \omega_o,\ b_0\}$ can stabilize the entire interval function family.

Note that the application of the Kharitonov theorem to calculate the stability regions of ADRC parameters is difficult because that the coefficients of Kharitonov functions are not independent and they influence each other when one of them changes.

To simplify the calculation of the stability region, the discussion about the stability region of ADRC in subsection 3.2 provides a method to calculate the stability region which can stabilize the entire interval function family.

Consider that the throttle opening position μ_t is selected to control the power output, take $g_{12}(s)$ in Equation (28) as an example to show the effectiveness of the proposed method. The operating ranges from A to G and from F to I are selected as the design range, and the scheduling range is from F to G as shown in Fig. 8. Based on the linearized model $g_{12}(s)$ in Equation (28) at selected operation conditions and the discussion in subsection 3.2, we can obtain the stability regions of ADRC with the fixed $b_0 = 1$ under the typical operation conditions (A, F, G, H, I) as shown in Fig. 11. We can know that the typical operation conditions (A, F, G, H, I) have the similar stability regions even though operation conditions very greatly. This verifies that the varying ADRC parameters in the scheduling ranges can locate in the stability region except that they locate near the stability boundaries where the ADRC parameters cannot ensure the satisfactory performance. Fig. 11 can also explain the rationality of the proposed gain scheduling design based on ADRC roughly.

5. Simulations results

In this section, simulations of the gain scheduling design based on ADRC with and without physical constraints of actuators such as amplitude limiting and rate limiting are carried out to verify the superiority of the proposed control strategy under full operating conditions. Note that the model and the proposed control strategy are built in *MATALB* and *Simulink*, and simulations are all carried out by *MATALB* language.

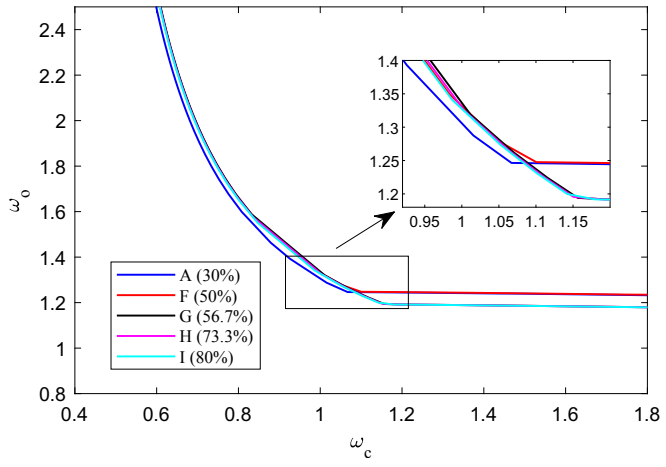

Fig. 11. The stability regions of ADRC under the typical operation conditions.

Based on the proposed control strategy discussed in Section 4, the control structure of the DEB combining with the gain scheduling design based on ADRC can be shown in Fig. 12 where the red part is the new content for the proposed control strategy. The proposed control strategy does not change the original structure and can reduce the implementation difficulty in DCS greatly by adding two parameters tables.

To design parameters Table 1 of the power output loop and Table 2 of the throttle pressure loop, parameters of the regular ADRC under the operating conditions A, E and G are tuned based on the tuning procedure shown in Fig. 4, respectively. Besides, the tuned parameters should be checked to ensure all of them locate in the stability region as discussed in subsection 3.2. Then the scheduling methods in Equations (34) and (35) are applied to the gain scheduling design based on ADRC. We can obtain parameters Table I and Table II as shown in Fig. 13. Besides, the feedforward PD controller $G_f(s)$ is $G_f(s) = 0.3 + 110s/(1 + 20s)$ and the fixed b_0 is equal to one for two control loops. The ADRC and the PI ($G_{PI}(s) = k_{p\_pi} + k_{i\_pi}/s$) control strategies are comparative control strategies and are tuned by the multi-objective parameter optimization. Their parameters are listed in Table 3 [38].

To better compare the control performance with different control strategies quantitatively, the integrated absolute error (IAE) and the control signal total variation (TV) are recorded which are depicted by

$$\mathrm{IAE}_i = \int_0^{\infty} |r_i(t) - y_i(t)| dt, \quad i = 1,\ 2 \tag{38}$$

$$\mathrm{TV}_i = \sum_{j=0}^{n-1} |u_i(j+1) - u_i(j)|, \quad i = 1,\ 2 \tag{39}$$

where $i = 1,\ 2$ for the power output loop and throttle pressure loop, respectively.

Firstly, we set the load tracking rate as 1.5% of full load per minute. Note that the simulation contains the full operating conditions from 30% (90 MW) to 100% (300 MW) where the system can experience the constant pressure operation and sliding pressure operation modes. The simulation results are shown in Fig. 14 - Fig. 17.

Without physical constraints of actuators, the gain scheduling design based on ADRC ("The Proposed" in figures) has the best control performance under full operating conditions and the PI ("PI" in figures)has the largest reverse change under sliding pressure operation mode and the largest deviation under constant pressure operation mode. Besides, the control signal of the proposed control strategy in Fig. 15 is flatter than that of the regular ADRC ("ADRC" in figures) and the PI. Similar conclusions can be obtained considering physical constraints of actuators as shown in Fig. 16 - Fig. 17. To show the results clearly, the local enlarged drawings of Figs. 16–17 from 35000s to 37000s are shown in Fig. 18 - Fig. 19, respectively, and the discussions above can be verified. Moreover, all control performance indices of these control strategies are recorded in Table 4. IAE of the proposed control strategy is about 50.6% and 82.8% of IAE of the regular ADRC in the power output loop and throttle pressure loop, respectively. Besides, IAE of the proposed control strategy is about 24.1% and 62.4% of IAE of the PI in the power output loop and throttle pressure loop, respectively. Therefore, the gain scheduling design based on ADRC can improve the control performance of power output and throttle pressure loops greatly.

During the process of load rising (0s–28000s), the overshoots of

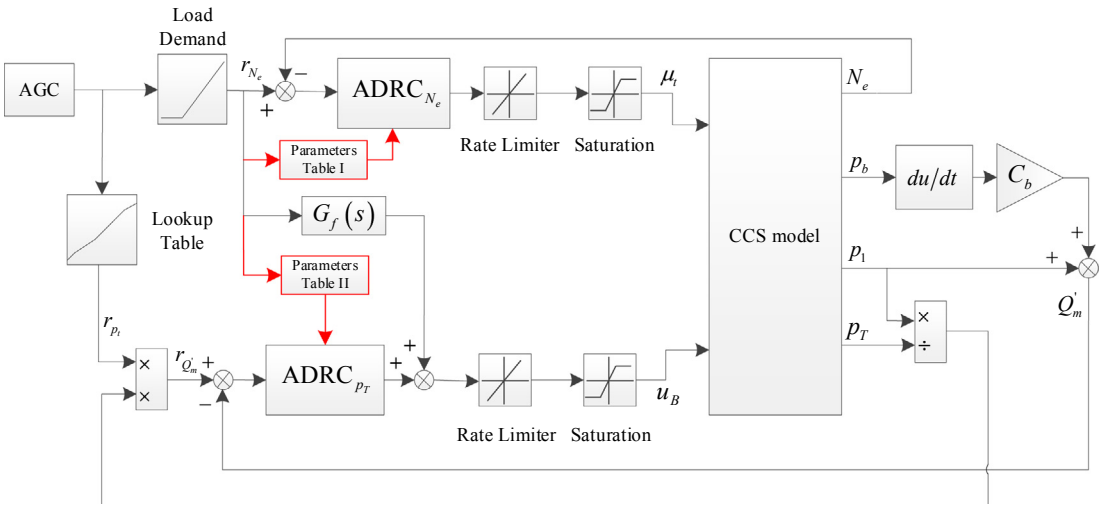

Fig. 12. The DEB control structure with the gain scheduling design based on ADRC.

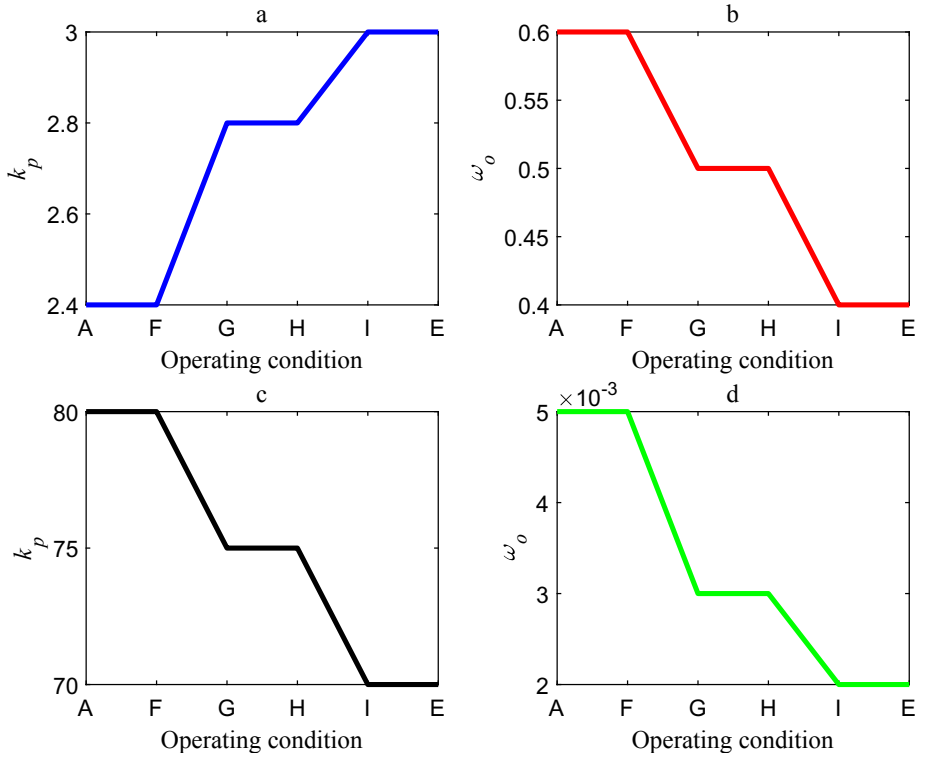

Fig. 13. The parameters of the ADRC for the gain scheduling design under different operating conditions. *((a),(b): the parameters of ADRC for the power output loop; (c),(d): the parameters of ADRC for the throttle pressure loop.).*

Table 3
Parameters of the comparative controllers.

Controllers	Parameters of different controllers
PI	$G_{N_{e\_c}}$: $k_{p\_pi} = 1.95$, $k_{i\_pi} = 0.11$; $G_{p_{T\_c}}$: $k_{p\_pi} = 69.1$, $k_{i\_pi} = 0.025$; $G_f(s) = 0.35 + \frac{7.84s}{52s+1}$;
ADRC	$G_{N_{e\_c}}$: $k_p = 1.95$, $\omega_o = 0.3$, $b_0 = 1$; $G_{p_{T\_c}}$: $k_p = 70$, $\omega_o = 0.002$, $b_0 = 1$; $G_f(s) = 0.3 + \frac{117s}{11.7s+1}$;

the power output loop with the proposed control strategy are 0.33%, 0.40%, 0.50%, 0.26%, 0.60%, 0.40% and 0.37%, respectively, with physical constraints of actuators. This means that the overshoot is relevant to the starting point caused by the nonlinearity of the CCS as discussed in subsection 2.2 and this is accord with the real power plants.

Note that the closed loop system with the PI has some severe operating conditions (the reverse change and the biggest deviation is larger than ± 0.4 MPa as discussed in subsection 2.1) as shown in green dashed boxes of Figs. 14 (b) and Fig. 16 (b). These may result in the irreversible damage for main steam pipes and bring the necessary manual interventions.

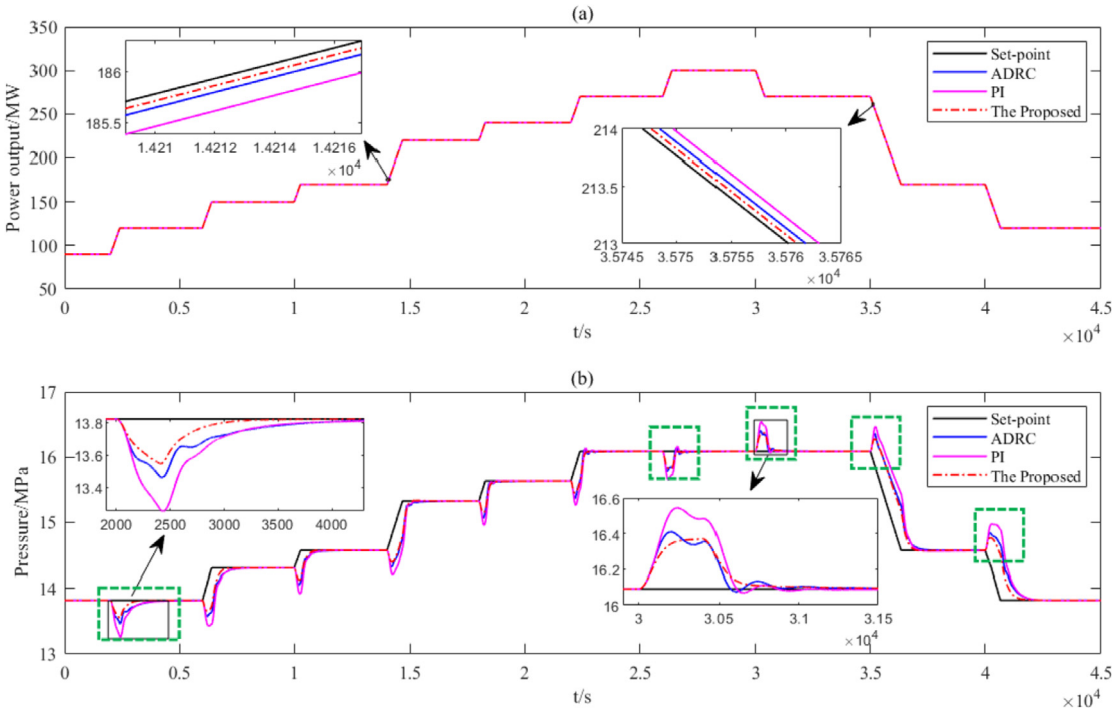

Fig. 14. The output responses of 1.5% load tracking rate without physical constraints of actuators. ((a): power output loop (b): throttle pressure loop).

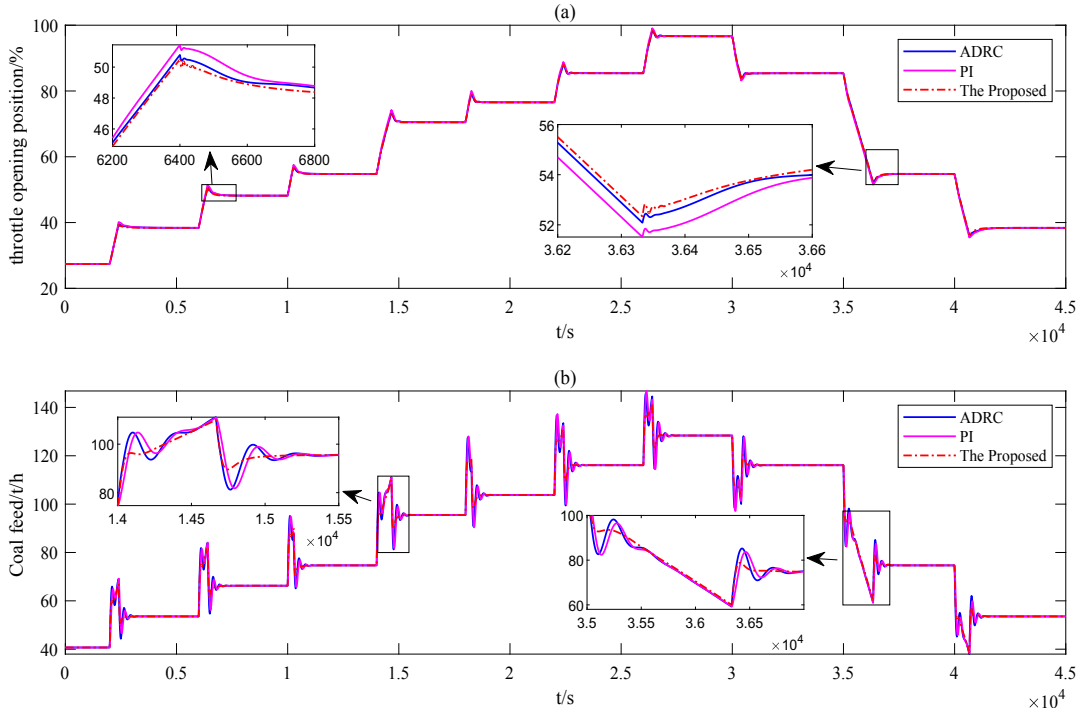

Fig. 15. The control signals of 1.5% load tracking rate without physical constraints of actuators. ((a): power output loop (b): throttle pressure loop).

To integrate more renewable energy into the power grid, the thermal power plant has to accelerate the power output responding the AGC command and the upper limit of the load tracking rate should be taken into consideration.

The simulation with the load tracking rate, 2% of full load per minute, is also carried out. All control performance indices of these control strategies with 2% load tracking rate are recorded in Table 5. Note that the PI cannot ensure the convergence and stability of two loops when physical constraints of actuators are considered as presented in Table 5. IAEs of the proposed control strategy are no more than 52.5% and 86.5% of IAE of the regular ADRC in the power output loop and throttle pressure loop, respectively. What is more, the closed loop system with the regular ADRC also has some severe operating conditions (the reverse change and the biggest deviation

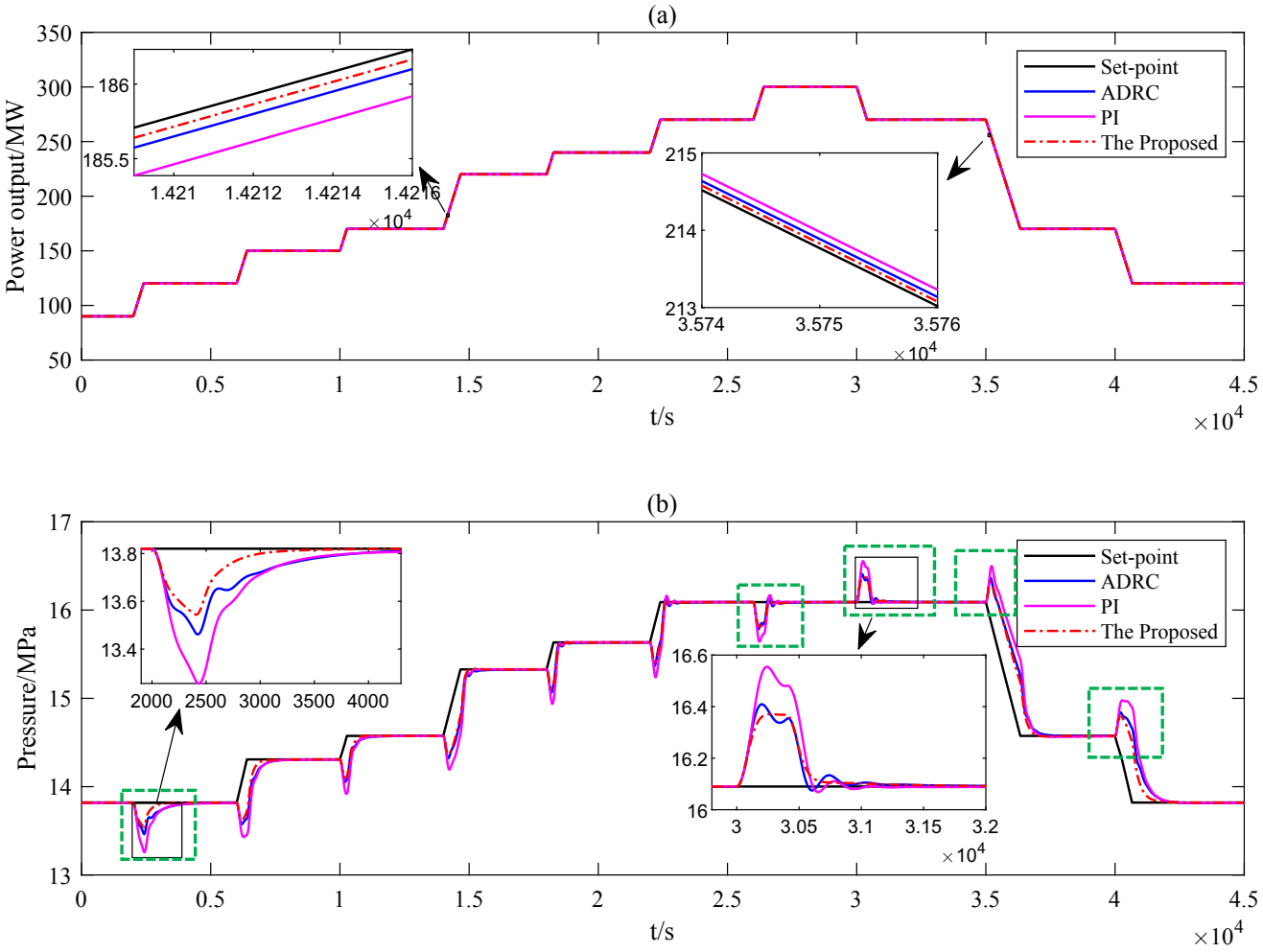

Fig. 16. The output responses of 1.5% load tracking rate with physical constraints of actuators. ((a): power output loop (b): throttle pressure loop).

is larger than ± 0.4 MPa as discussed in subsection 2.1) where the regular ADRC can result in irreversible damage for main steam pipes and bring the necessary manual interventions. However, the proposed control strategy still has no severe operating conditions which means that the proposed control strategy still has approving control performance when the system has a larger load tracking rate under full operating conditions.

Generally, the proposed control strategy can improve the control quality significantly while the PI is not competent the task for the large load tracking rate and the regular ADRC has poor control quality.

Now the concern goes to the issue of coal quality variation. Since k_c in Equation (2) is the index of the coal quality, to imitate the step and periodic disturbance of coal quality variation, the test can be done by increasing k_c by 20% at 500 s and oscillating k_c at 5000 s with the period of 628s under the typical operating condition D (90%) in Table 1. Simulation results are shown in Fig. 20 - Fig. 21. Note that the test is carried out with physical constraints of actuators in Equation (8).

The proposed control strategy can obtain best disturbance rejection no matter which type of coal quality variation as shown in Figs. 20–21. Moreover, the disturbance rejection indices of these control strategies are recorded in Table 6 and the indices verify the superiority of the proposed control strategy in disturbance rejection. The disturbance rejection indices under the operating condition G (56.7%) are also recorded in Table 6, and we can learn that the proposed control strategy still works best under other operating conditions.

Based on simulation results of the tracking performance with different load tracking rates and disturbance performance with the coal quality variation, the proposed control strategy can obtain the best control performance compared to the regular ADRC and the PI which are tuned by the multi-objective parameter optimization. The successful comparison indicates a promising future of the gain scheduling design based on ADRC for thermal power plants with the increasing demand on integrating more renewable energy into the power grid.

6. Conclusions

The renewable energy which has strong intermittency and randomness is playing an increasingly significant role in energy supply. To integrate more renewable energy into the grid, the thermal power plant has to accelerate the speed of power output responding the AGC command and enlarge its operating range. This puts forward great challenges on the safe operation and the control of thermal power plant. To this end, the gain scheduling design based on ADRC is proposed for the thermal power plant under full operating conditions from 30% to 100% of full load considering the constant and sliding pressure operation modes. The main work in this paper can be summarized as follows: 1) The necessary and importance of the proposed control strategies is discussed by

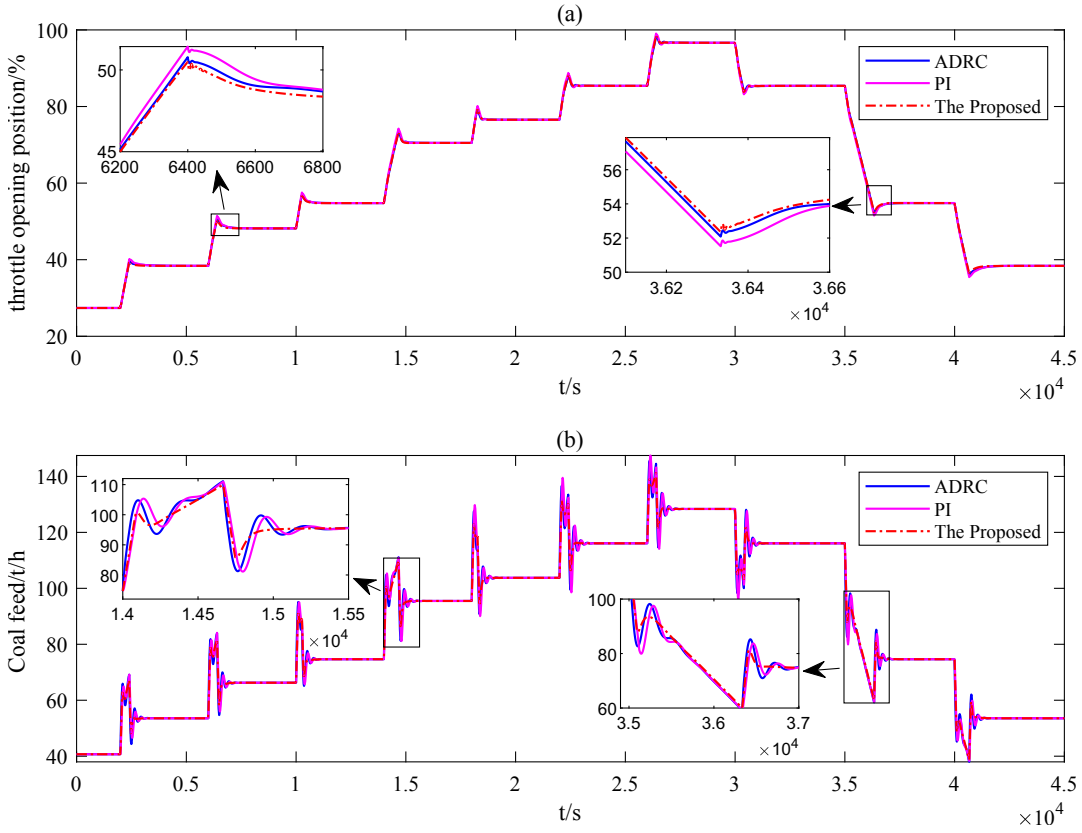

Fig. 17. The control signals of 1.5% load tracking rate with physical constraints of actuators. ((a): power output loop (b): throttle pressure loop).

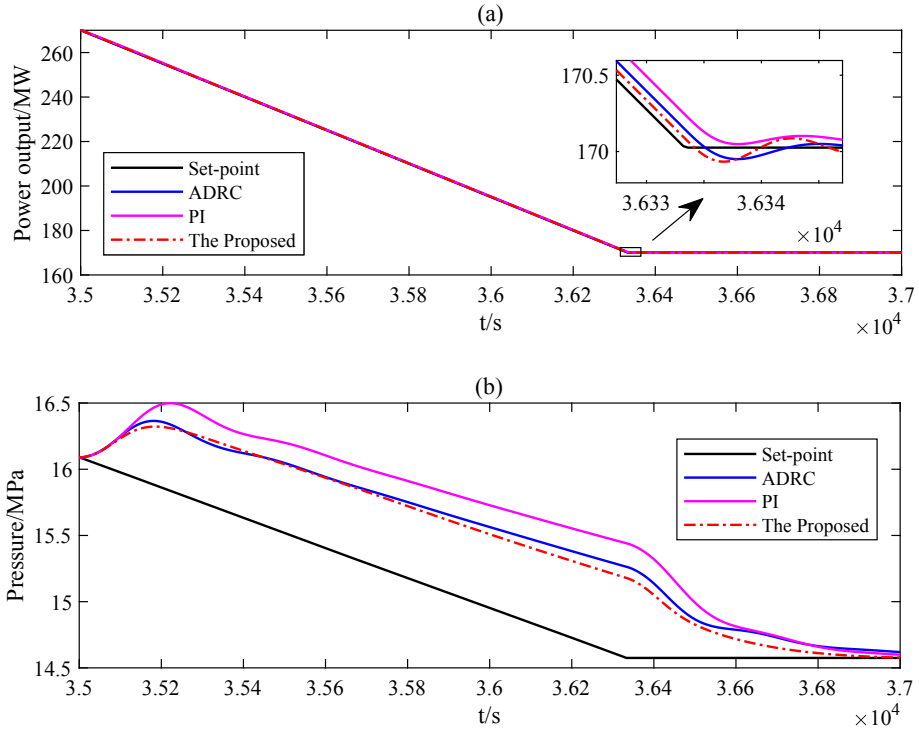

Fig. 18. The local enlarged drawing of Fig. 16 from 35000s to 37000s.

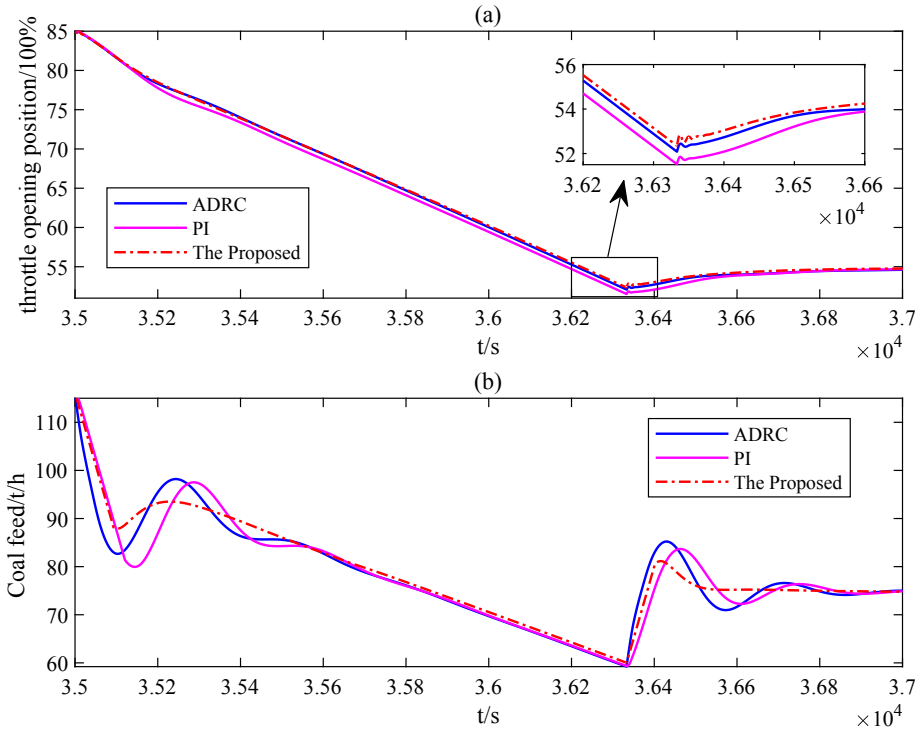

Fig. 19. The local enlarged drawing of Fig. 17 from 35000s to 37000s.

Table 4
The control performance indices of different control strategies under 1.5% load tracking rate.

Controllers		IAE_1	IAE_2	TV_1	TV_2
Without	PI	1669.8	4379.8	192.9	998.7
	ADRC	794.5	3301.5	180.1	1093.7
	The Proposed	402.0	2734.9	186.1	557.6
With	PI	1674.3	4395.3	193.4	1034.1
	ADRC	794.5	3301.5	180.1	1093.7
	The Proposed	402.6	2737.2	186.7	681.0

(Note that “Without” and “With” mean without and with physical constraints of actuators, respectively.)

Table 5
The control performance indices of different control strategies under 2% load tracking rate.

Controllers		IAE_1	IAE_2	TV_1	TV_2
Without	PI	19515.2	44500.0	211.8	1214.9
	ADRC	8366.0	33233.0	194.4	1334.5
	The Proposed	4209.3	27627.1	203.2	693.2
With	PI	3.1902×10^6	7.9742×10^5	1758.0	5183.9
	ADRC	8366.0	33233.5	194.4	1.334.6
	The Proposed	4389.4	28751.3	220.3	1084.5

(Note that “Without” and “With” mean without and with physical constraints of actuators, respectively.)

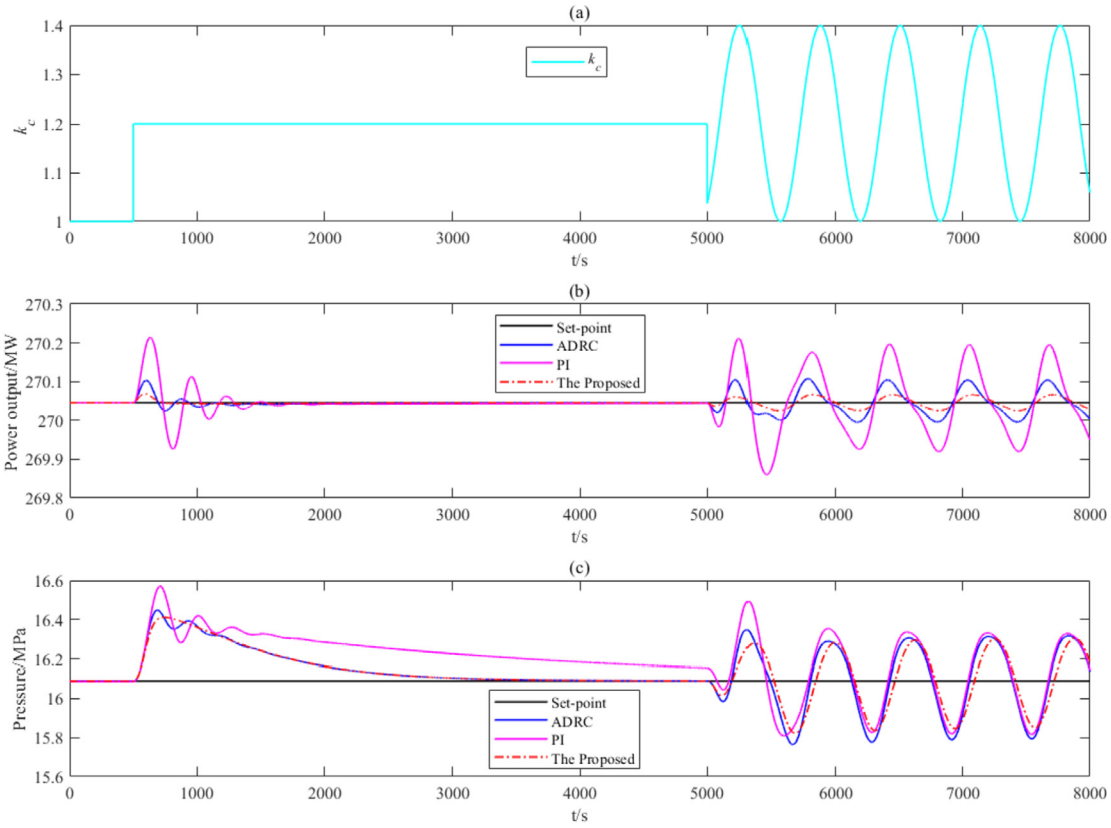

Fig. 20. The output responses in response to the coal quality variation under 90% load. ((a): the disturbance of coal quality variation (b): power output loop (c): throttle pressure loop).

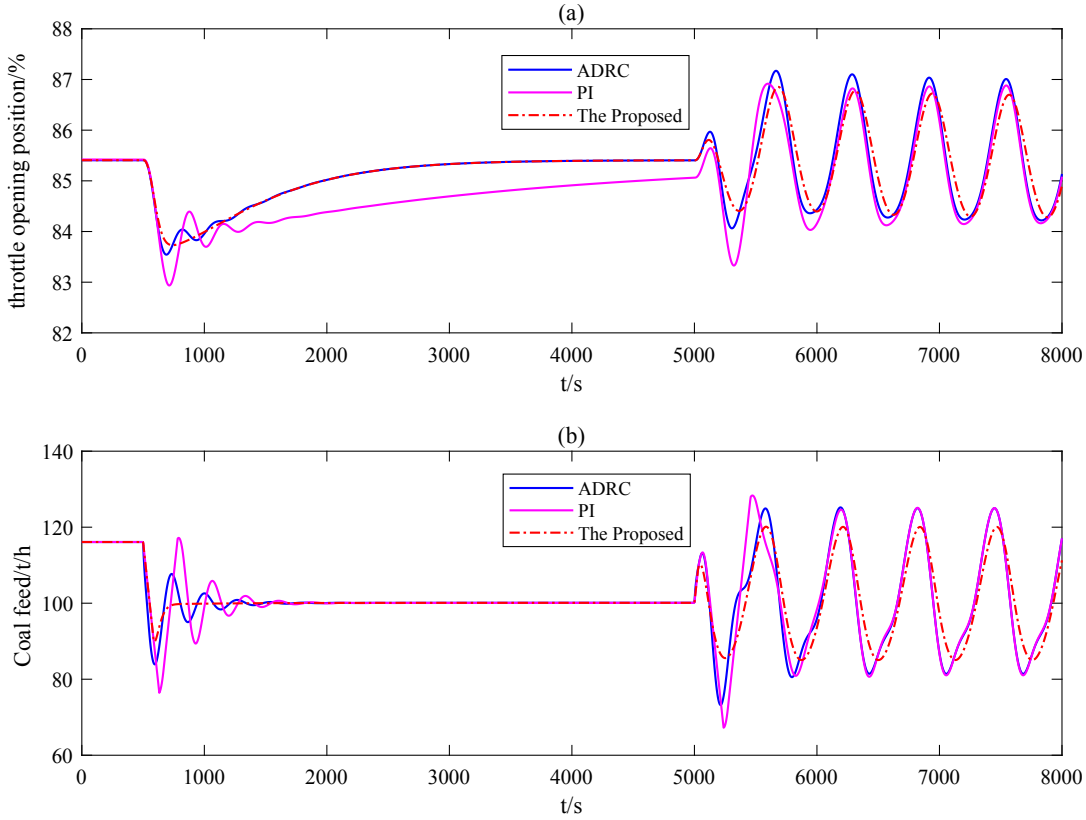

Fig. 21. The control signals in response to the coal quality variation under 90% load. ((a): power output loop (b): throttle pressure loop).

Table 6
The indices with the coal quality variation under operating conditions D and G.

Controllers		IAE_1	IAE_2	TV_1	TV_2
90%	PI	2934.8	13281.4	33.2	614.0
	ADRC	1026.5	8073.9	30.1	533.8
	The Proposed	418.2	7382.9	25.2	377.1
56.7%	PI	1096.3	11125.2	12.3	294.1
	ADRC	430.6	6096.8	12.6	291.0
	The Proposed	147.1	4375.0	10.3	213.8

analyzing the control difficulties of the CCS. 2) The gain scheduling design based on ADRC under full operating conditions about the scheduling parameter selection and division of operating conditions is discussed. 3) A linear switching method of the observer bandwidth ω_o and controller bandwidth ω_c is derived, the stability analysis based on the Kharitonov theorem is carried out qualitatively and the stability regions with different operating conditions are discussed quantitatively. 4) Simulations of power tracking with different load tracking rates and disturbance rejection with the coal quality variation are carried out to verify the superiority of the proposed control strategy under full operating conditions compared to the regular ADRC and the PI. The theoretical analysis and successful comparison indicate a promising potential for application to thermal power plant.

Acknowledgement

This work was supported by National Natural Science Foundation of China under Grant No.51876096, National Key Research and Development Program of China under Grant No.2016YFB0901405 and State Key Lab of Power Systems. The first author also would like to give thanks to the China Scholarship Council (CSC), Grant 201806210219, for funding towards research at University of California, Merced.

Appendix A

$$T_i(s)=b_0\lambda_1 s^3+(k_{p\_i}\alpha_1+b_0+b_0\omega_{o\_i}\lambda_1)s^2+\left(b_0\omega_{o\_i}+\omega_{o\_i}^2\alpha_1+2k_{p\_i}\omega_{o\_i}\alpha_1\right)s+k_{p\_i}\omega_{o\_i}^2\alpha_1 \tag{A-1}$$

$$T_{i+1}(s)=b_0\lambda_1 s^3+\left(k_{p\_i+1}\alpha_1+b_0+b_0\omega_{o\_i+1}\lambda_1\right)s^2+\left(b_0\omega_{o\_i+1}+\omega_{o\_i+1}^2\alpha_1+2k_{p\_i+1}\omega_{o\_i+1}\alpha_1\right)s+k_{p\_i+1}\omega_{o\_i+1}^2\alpha_1 \tag{A-2}$$

$$b_0\lambda_1>0 \tag{A-3}$$

$$k_{p\_i}\alpha_1+b_0+b_0\omega_{o\_i}\lambda_1>0 \tag{A-4}$$

$$b_0\omega_{o\_i}+\omega_{o\_i}^2\alpha_1+2k_{p\_i}\omega_{o\_i}\alpha_1>0 \tag{A-5}$$

$$k_{p\_i}\omega_{o\_i}^2\alpha_1>0 \tag{A-6}$$

$$(k_{p\_i}\alpha_1+b_0+b_0\omega_{o\_i}\lambda_1)k_{p\_i}\omega_{o\_i}^2\alpha_1>\left(b_0\omega_{o\_i}+\omega_{o\_i}^2\alpha_1+2k_{p\_i}\omega_{o\_i}\alpha_1\right)b_0\lambda_1 \tag{A-7}$$

$$k_{p\_i+1}\alpha_1+b_0+b_0\omega_{o\_i+1}\lambda_1>0 \tag{A-8}$$

$$b_0\omega_{o\_i+1}+\omega_{o\_i+1}^2\alpha_1+2k_{p\_i+1}\omega_{o\_i+1}\alpha_1>0 \tag{A-9}$$

$$k_{p\_i+1}\omega_{o\_i+1}^2\alpha_1>0 \tag{A-9}$$

$$\left(k_{p\_i+1}\alpha_1+b_0+b_0\omega_{o\_i+1}\lambda_1\right)k_{p\_i+1}\omega_{o\_i+1}^2\alpha_1>\left(b_0\omega_{o\_i+1}+\omega_{o\_i+1}^2\alpha_1+2k_{p\_i+1}\omega_{o\_i+1}\alpha_1\right)b_0\lambda_1 \tag{A-10}$$

$$G_{c^*}(s)=\frac{\left[\varphi k_{p\_i}+(1-\varphi)k_{p\_i+1}\right]s^2}{\left[s+2\varphi\omega_{o\_i}+2(1-\varphi)\omega_{o\_i+1}\right]b_0 s}+\frac{\left\{\begin{array}{l}\left[\varphi\omega_{o\_i}+(1-\varphi)\omega_{o\_i+1}\right]^2+\\2\left[\varphi k_{p\_i}+(1-\varphi)k_{p\_i+1}\right]\left[\varphi\omega_{o\_i}+(1-\varphi)\omega_{o\_i+1}\right]\end{array}\right\}s}{\left[s+2\varphi\omega_{o\_i}+2(1-\varphi)\omega_{o\_i+1}\right]b_0 s}+\frac{\left[\varphi k_{p\_i}+(1-\varphi)k_{p\_i+1}\right]\left[\varphi\omega_{o\_i}+(1-\varphi)\omega_{o\_i+1}\right]^2}{\left[s+2\varphi\omega_{o\_i}+2(1-\varphi)\omega_{o\_i+1}\right]b_0 s} \tag{A-11}$$

$$T_{i^*}(s)=b_0\lambda_1 s^3+\left\{\left[\phi k_{p\_i}+(1-\phi)k_{p\_i+1}\right]\alpha_1+b_0+b_0\left[\phi\omega_{o\_i}+(1-\phi)\omega_{o\_i+1}\right]\lambda_1\right\}s^2+\left\{\begin{array}{l}b_0\left[\phi\omega_{o\_i}+(1-\phi)\omega_{o\_i+1}\right]+\left[\phi\omega_{o\_i}+(1-\phi)\omega_{o\_i+1}\right]^2\alpha_1\\+2\left[\phi k_{p\_i}+(1-\phi)k_{p\_i+1}\right]\left[\phi\omega_{o\_i}+(1-\phi)\omega_{o\_i+1}\right]\alpha_1\end{array}\right\}s+\left[\phi k_{p\_i}+(1-\phi)k_{p\_i+1}\right]\left[\phi\omega_{o\_i}+(1-\phi)\omega_{o\_i+1}\right]^2\alpha_1 \tag{A-12}$$

$$\left\{\left[\varphi k_{p\_i}+(1-\varphi)k_{p\_i+1}\right]\alpha_1+b_0+b_0\left[\varphi\omega_{o\_i}+(1-\varphi)\omega_{o\_i+1}\right]\lambda_1\right\}\times\left[\varphi k_{p\_i}+(1-\varphi)k_{p\_i+1}\right]\left[\varphi\omega_{o\_i}+(1-\varphi)\omega_{o\_i+1}\right]^2\alpha_1 > \left\{\begin{array}{l} b_0\left[\varphi\omega_{o\_i}+(1-\varphi)\omega_{o\_i+1}\right]+\left[\varphi\omega_{o\_i}+(1-\varphi)\omega_{o\_i+1}\right]^2\alpha_1 \\ +2\left[\varphi k_{p\_i}+(1-\varphi)k_{p\_i+1}\right]\left[\varphi\omega_{o\_i}+(1-\varphi)\omega_{o\_i+1}\right]\alpha_1 \end{array}\right\}b_0\lambda_1 \tag{A-13}$$

Appendix B

$$T(s)=k_p\omega_o^2n_0+\left(k_p\omega_o^2n_1+2k_p\omega_on_0+2\omega_ob_o+\omega_o^2n_0\right)s+\left(b_0+2\omega_ob_od_1+\omega_o^2n_1+2k_p\omega_on_1+k_p\omega_o^2n_2+k_pn_0\right)s^2+\left(b_od_1+2\omega_ob_od_2+k_pn_1+\omega_o^2n_2+2k_p\omega_on_2+k_p\omega_o^2n_3\right)s^3+\left(b_od_2+2\omega_ob_od_3+k_pn_2+\omega_o^2n_3+2k_p\omega_on_3\right)s^4+(b_od_3+2\omega_ob_od_4+k_pn_3)s^5+b_od_4s^6 \tag{B-1}$$

$$T_1(s)=A_{0\_\min}+A_{1\_\min}s+A_{2\_\max}s^2+A_{3\_\max}s^3+A_{4\_\min}s^4+A_{5\_\min}s^5+A_{6\_\max}s^6 \tag{B-2}$$

$$T_2(s)=A_{0\_\max}+A_{1\_\min}s+A_{2\_\min}s^2+A_{3\_\max}s^3+A_{4\_\max}s^4+A_{5\_\min}s^5+A_{6\_\min}s^6 \tag{B-3}$$

$$T_3(s)=A_{0\_\max}+A_{1\_\max}s+A_{2\_\min}s^2+A_{3\_\min}s^3+A_{4\_\max}s^4+A_{5\_\max}s^5+A_{6\_\min}s^6 \tag{B-4}$$

$$T_4(s)=A_{0\_\min}+A_{1\_\max}s+A_{2\_\max}s^2+A_{3\_\min}s^3+A_{4\_\min}s^4+A_{5\_\max}s^5+A_{6\_\max}s^6 \tag{B-5}$$

The expressions of $A_{0\_\min}$, $A_{0\_\max}$ et al. are listed as follows,

$$A_{0\_\min}=k_p\omega_o^2n_{0\min},$$

$$A_{0\_\max}=k_p\omega_o^2n_{0\max},$$

$$A_{1\_\min}=k_p\omega_o^2n_{1\min}+2k_p\omega_on_{0\min}+2\omega_ob_o+\omega_o^2n_{0\min},$$

$$A_{1\_\max}=k_p\omega_o^2n_{1\max}+2k_p\omega_on_{0\max}+2\omega_ob_o+\omega_o^2n_{0\max},$$

$$A_{2\_\min}=b_0+2\omega_ob_od_{1\min}+\omega_o^2n_{1\min}+2k_p\omega_on_{1\min}+k_p\omega_o^2n_{2\min}+k_pn_{0\min},$$

$$A_{2\_\max}=b_0+2\omega_ob_od_{1\max}+\omega_o^2n_{1\max}+2k_p\omega_on_{1\max}+k_p\omega_o^2n_{2\max}+k_pn_{0\max},$$

$$A_{3\_\min}=b_od_{1\min}+2\omega_ob_od_{2\min}+k_pn_{1\min}+\omega_o^2n_{2\min}+2k_p\omega_on_{2\min}+k_p\omega_o^2n_{3\min},$$

$$A_{3\_\max}=b_od_{1\max}+2\omega_ob_od_{2\max}+k_pn_{1\max}+\omega_o^2n_{2\max}+2k_p\omega_on_{2\max}+k_p\omega_o^2n_{3\max},$$

$$A_{4\_\min}=b_od_{2\min}+2\omega_ob_od_{3\min}+k_pn_{2\min}+\omega_o^2n_{3\min}+2k_p\omega_on_{3\min},$$

$$A_{4\_\max}=b_od_{2\max}+2\omega_ob_od_{3\max}+k_pn_{2\max}+\omega_o^2n_{3\max}+2k_p\omega_on_{3\max},$$

$$A_{5\_\min}=b_od_{3\min}+2\omega_ob_od_{4\min}+k_pn_{3\min},$$

$$A_{5\_\max}=b_od_{3\max}+2\omega_ob_od_{4\max}+k_pn_{3\max},$$

$$A_{6\_\min}=b_od_{4\min},$$

$$A_{6\_\max}=b_od_{4\max}.$$

References

[1] Nahla Alamoodi, Prodromos Daoutidis. Nonlinear decoupling control with deadtime compensation for multirange operation of steam power plants. IEEE Trans Control Syst Technol 2016;24(1):341–8.
[2] Wu Zhenlong, He Ting, Sun Li, Li Donghai, Xue yali. The facilitation of a sustainable power system: a practice from data-driven enhanced boiler control. Sustainability 2018;10(4):1112.
[3] Alberto Benato, Stefano Bracco, Anna Stoppato, Alberto Mirandola. LTE: a procedure to predict power plants dynamic behaviour and components lifetime reduction during transient operation. Appl Energy 2016;162:880–91.
[4] Alberto Benato, Anna Stoppato, Alberto Mirandola, Destro Nicola, Bracco Stefano. Superheater and drum lifetime estimation: an approach based on dynamic analysis. J Energy Resour Technol 2017;139(3):031001.
[5] Sun Li, Li Donghai, Lee Kwang Y. Optimal disturbance rejection for PI controller with constraints on relative delay margin. ISA (Instrum Soc Am) Trans 2016;63:103–11.
[6] Wu Xiao, Shen Jiong, Li Yiguo, Lee Kwang Y. Steam power plant configuration, design, and control. Wiley Interdisciplinary Reviews: Energy Environ 2015;4(6):537–63.
[7] Moritz Hübel, Sebastian Meinke, Andrén Marcus T, Christoffer Wedding, Jürgen Nocke, Conrad Gierow, Egon Hassel, Jonas Funkquistc. Modelling and simulation of a coal-fired power plant for start-up optimization. Appl Energy 2017;208:319–31.
[8] Alberto Benato, Stefano Bracco, Anna Stoppato, Alberto Mirandola. Dynamic simulation of combined cycle power plant cycling in the electricity market. Energy Convers Manag 2016;107:76–85.
[9] Alberto Benato, Anna Stoppato, Stefano Bracco. Combined cycle power plants: a comparison between two different dynamic models to evaluate transient behaviour and residual life. Energy Convers Manag 2014;87:1269–80.
[10] Alberto Benato, Anna Stoppato, Alberto Mirandola. Dynamic behaviour analysis of a three pressure level heat recovery steam generator during transient operation. Energy 2015;90:1595–605.
[11] Alberto Benato, Kærn Kærn, Leonardo Pierobon, Stoppato Ann, Fredrik Haglind. Analysis of hot spots in boilers of organic Rankine cycle units during transient operation. Appl Energy 2015;151:119–31.
[12] Long Dongteng, Wang Wei, Yao Chu, Liu Jizhen. An experiment-based model of condensate throttling and its utilization in load control of 1000 MW power units. Energy 2017;133:941–54.
[13] Åström KJ, Bell RD. Drum-boiler dynamics. Automatica 2000;36(3):363–78.
[14] Liu Jizhen, Shu Yan, Zeng Deliang, Hu Yong, You Lv. A dynamic model used for controller design of a coal fired once-through boiler-turbine unit. Energy 2015;93:2069–78.
[15] Sun Li, Li Donghai, Lee Kwang Y, Xue Yali. Control-oriented modeling and

analysis of direct energy balance in coal-fired boiler-turbine unit. Contr Eng Pract 2016;55:38–55.
[16] Maciej Ławryńczuk. Nonlinear predictive control of a boiler-turbine unit: a state-space approach with successive on-line model linearisation and quadratic optimisation. ISA (Instrum Soc Am) Trans 2017;67:476–95.
[17] Liu Xiangjie, Cui Jinghan. Economic model predictive control of boiler-turbine system. J Process Control 2018;66:59–67.
[18] Hamed Moradi, Aria Alasty, Gholamreza Vossoughi. Nonlinear dynamics and control of bifurcation to regulate the performance of a boiler–turbine unit. Energy Convers Manag 2013;68:105–13.
[19] Zhou Hong, Cheng Chen, Lai Jingang, Lu Xiaoqing, Deng Qijun, Gao Xingran, Lei Zhongcheng. Affine nonlinear control for an ultra-supercritical coal fired once-through boiler-turbine unit. Energy 2018;153:638–49.
[20] Piraisoodi T, Willjuice Iruthayarajan M, Mohaideen Abdul Kadhar K. An optimized nonlinear controller design for boiler–turbine system using evolutionary algorithms. IETE J Res 2018;64(4):451–62.
[21] Mohammad Ataei, Rahmat-Allah Hooshmand, Golmohammadi Samani Siavash. A coordinated MIMO control design for a power plant using improved sliding mode controller. ISA (Instrum Soc Am) Trans 2014;53(2):415–22.
[22] Soheil Ghabraei, Hamed Moradi, Gholamreza Vossoughi. Multivariable robust adaptive sliding mode control of an industrial boiler–turbine in the presence of modeling imprecisions and external disturbances: a comparison with type-I servo controller. ISA (Instrum Soc Am) Trans 2015;58:398–408.
[23] Vincenzo Iannino, Valentina Colla, Mario Innocenti, Annamaria Signorini. Design of a H∞ robust controller with μ-analysis for steam turbine power generation applications. Energies 2017;10(7):1026.
[24] Un-Chul Moon, Lee Youngjun, Lee Kang Y. Practical dynamic matrix control for thermal power plant coordinated control. Contr Eng Pract 2018;71:154–63.
[25] Lei Yu, Lim Jae Gyoung, Fei Shumin. An improved single neuron self-adaptive PID control scheme of superheated steam temperature control system. International Journal of System Control and Information Processing 2017;2(1):1–13.
[26] Ma Liangyu, Wang Zhiyan, Lee Kwang Y. Neural network inverse control for the coordinated system of a 600MW supercritical boiler unit. IFAC Proceedings Volumes 2014;47(3):999–1004.
[27] Wang Wei, Liu Jizhen, Zeng Deliang, Niu Yuguang, Cui Can. An improved coordinated control strategy for boiler-turbine units supplemented by cold source flow adjustment. Energy 2015;88:927–34.
[28] Han Jinqing. From PID to active disturbance rejection control. IEEE Trans Ind Electron 2009;56(3):900–6.
[29] Madoński R, Herman P. Survey on methods of increasing the efficiency of extended state disturbance observers. ISA (Instrum Soc Am) Trans 2015;56:18–27.
[30] Zhang Yuqiong, Li Donghai, Gao Zhiqiang, Zheng Qinling. On oscillation reduction in feedback control for processes with an uncertain dead time and internal–external disturbances. ISA (Instrum Soc Am) Trans 2015;59:29–38.
[31] Huang Yi, Xue Wenchao. Active disturbance rejection control: methodology and theoretical analysis. ISA (Instrum Soc Am) Trans 2014;53(4):963–76.
[32] Feng Hongyinping, Guo Baozhu. Active disturbance rejection control: old and new results. Annu Rev Contr 2017;44:238–48.
[33] Yuan Yuan, Wang Zidong, Yang Yu, Guo Lei, Yang Hongjiu. Active disturbance rejection control for a pneumatic motion platform subject to actuator saturation: an extended state observer approach. Automatica 2019;107:353–61.
[34] Kang Song, Tianyuan Hao, Xie Hui. Disturbance rejection control of air–fuel ratio with transport-delay in engines. Contr Eng Pract 2018;79:36–49.
[35] Zheng Qinling, Zhan Ping, Soares Simone, Hu Yu, Gao Zhiqiang. An optimized active disturbance rejection approach to fan control in server. Contr Eng Pract 2018;79:154–69.
[36] Shi Rongqi, He Tianqi, Peng Jie, Zhang Yangjun, Zhuge Weilin. System design and control for waste heat recovery of automotive engines based on Organic Rankine Cycle. Energy 2016;102:276–86.
[37] Xia Yuanqing, Liu Bo, Fu Mengyin. Active disturbance rejection control for power plant with a single loop. Asian J Contr 2012;14(1):239–50.
[38] Sun Li, Hua Qingsong, Li Donghai, Pan Lei, Xue Yali, Lee Kwang Y. Direct energy balance based active disturbance rejection control for coal-fired power plant. ISA (Instrum Soc Am) Trans 2017;70:486–93.
[39] Rugh Wilson J, Shamma Jeff S. Research on gain scheduling. Automatica 2000;36(10):1401–25.
[40] Dounis Anastasios I, Panagiotis Kofinas, Constantine Alafodimos, Tseles Dimitrios. Adaptive fuzzy gain scheduling PID controller for maximum power point tracking of photovoltaic system. Renew Energy 2013;60:202–14.
[41] Huang Deqing, Jian-xu Xu, Venkatakrishnan Venkataramanan, Tuong Huynhet. High-performance tracking of piezoelectric positioning stage using current-cycle iterative learning control with gain scheduling. IEEE Trans Ind Electron 2013;61(2):1085–98.
[42] Yang Yueneng, Ye Yan. Attitude regulation for unmanned quadrotors using adaptive fuzzy gain-scheduling sliding mode control. Aero Sci Technol 2016;54:208–17.
[43] Gallego Antonio J, Merello Gonzalo M, Manuel Berenguel, Camacho Eduardo F. Gain-scheduling model predictive control of a Fresnel collector field. Contr Eng Pract 2019;82:1–13.
[44] Tan Wan, Marquez Horacio J, Chen Tongwen, Liu Jizhen. Analysis and control of a nonlinear boiler-turbine unit. J Process Control 2005;15(8):883–91.
[45] Wu Xiao, Shen Jiong, Li Yiguo, Lee Kwang Y. Fuzzy modeling and stable model predictive tracking control of large-scale power plants. J Process Control 2014;24(10):1609–26.
[46] Zhao Chunzhe, Li Donghai. Control design for the SISO system with the unknown order and the unknown relative degree. ISA (Instrum Soc Am) Trans 2014;53(4):858–72.
[47] Wu Zhenlong, He Ting, Li Donghai, Xue Yali, Sun Li, Sun Liming. Superheated steam temperature control based on modified active disturbance rejection control. Contr Eng Pract 2019;83:83–97.
[48] Li Mingda, Li Dognhai, Wang Jing, Zhao Chunzhe. Active disturbance rejection control for fractional-order system. ISA (Instrum Soc Am) Trans 2013;52(3):365–74.
[49] Gao Zhiqiang. Scaling and bandwidth-parameterization based controller tuning. Proceedings of the American control conference (ACC), vol. 6; June 4-6; 2006. p. 4989–96. Denver, CO, USA.
[50] Xue Wenchao, Huang Yi. Performance analysis of active disturbance rejection tracking control for a class of uncertain LTI systems. ISA (Instrum Soc Am) Trans 2015;58:133–54.
[51] Wu Zhenlong, He Ting, Li Donghai, Xue Yali. The calculation of stability and robustness regions for active disturbance rejection controller and its engineering application. Control Theory & Appl 2018;35(11):1635–47.
[52] Mehrdad Pakmehr, Nathan Fitzgerald, Feron Eric M, Shamma Jeff S, Alireza Behbahani. Gain scheduled control of gas turbine engines: stability and verification. J Eng Gas Turbines Power 2014;136(3):031201.
[53] Chapellat H, Bhattacharyya SP. A generalization of Kharitonov's theorem; Robust stability of interval plants. IEEE Trans Autom Control 1989;34(3):306–11.